Autogenic signals in an experimental source-to-sink system

A Thesis
SUBMITTED TO THE FACULTY OF
UNIVERSITY OF MINNESOTA
BY

Edward William Gazzetti

IN PARTIAL FULFILLMENT OF THE REQUIREMENTS
FOR THE DEGREE OF
MASTER OF SCIENCE

Dr. John B Swenson

December, 2015

Acknowledgements

Dedication

This thesis is dedicated to my family. You have given me so much support and I am truly grateful. I wouldn't be where I am today without your guidance and love. Mom, thank you for raising us to be good people. Thank you for working so hard to put food on the table and a roof over our head. You did it alone most of the time which makes it so much more impressive. When we were young, we didn't realize how difficult that must have been. As an adult, I am amazed by the sacrifices you made and the miracles you performed. Thanks to Steven and Megan for being such great siblings. Steve, you have always been there for me, showing me unconditional love. You're my big brother and I've always looked up to you. Thanks for not getting mad at me for copying you over the years (your clothes, your friends, your hobbies, etc.). Megan, you are the spark in our family and I hope you never change. You provide us all with energy, hope and happiness. You're honest and kind and everyone (yes, everyone) loves being around you, including myself. I couldn't ask for a better sister. Dad, thank you for coming back into our lives. We have a lot to gain from your kindness and patience. I hope you've found a new home in upstate NY. Papa, you've shown me what it means to be a good man. You've always been there for our family, providing support when we needed it most. I'll always look to you for advice. Please tell Thomas that I thank him for all his help. Virginia, you inspire me to be a better person. You were my rock even when you didn't know it. I'm very grateful for our time in Duluth, where we started our story by putting blood, sweat, and tears into our work.

Thank you all so much for the inspiration, love and support you have given me. I only hope that I can repay you someday. I love you all very much.

Abstract

Interpretations of the sedimentary rock record typically focus on allogenic forcing like fluctuations in relative sea-level and autogenic processes like fluvial avulsions and delta-lobe switching within the depositional system. I investigated the potential for drainage-basin-derived autogenic variability in sediment discharge to be preserved in the sedimentary rock record. I constructed a source-to-sink experimental apparatus to study the development of autogenic variability 'signals' in a net-erosional drainage basin and to trace these autogenic signals to a connected net-depositional basin (the 'sink'), where they are preserved in a prograding fluvo-deltaic system. By maintaining constant tectonic uplift rate, climate (precipitation rate), and rock strength, I attempted to isolate and measure how allogenic forcing generates autogenic signals in the source terrane. Experimental results suggest that the interaction of landslides with channel processes in the drainage basin generates sediment-discharge variability. The scale of experimental landsliding is set by ridge relief, and landscapes with high rock strength, high uplift rate, and low precipitation rate have the potential to generate high-relief ridges. Thus, these systems can generate relatively large autogenic variability (+/- 10% from the mean) in sediment discharge. These experiments suggest that this autogenic variability in sediment supply propagates through the net-depositional fluvial system with minor time lags and can be preserved in the deltaic strata.

Table of Contents

List of Tables

List of Figures

1. INTRODUCTION

The sedimentary record is a complicated and tangled timeline of geologic events. It is a product of allogenic (externally forced) and autogenic (self-organized) processes that occur from source to sink, throughout the entire sediment routing system. Typically, when the rock record is inverted to reconstruct past environments, allogenic controls like sea-level, tectonic uplift, and climate are considered the predominant causal mechanisms. There is no doubt that these controls do, indeed, play a major role in the composition of the sedimentary record; yet, autogenic processes must also be considered, particularly in strata that record deposition on smaller time scales, e.g. 'parasequences' (Van Wagoner et al., 1990).

Untangling autogenic and allogenic signals from sedimentary rocks is a daunting task. Yet, the ability to decouple these is essential in the reconstruction of paleo-environments. In order to further our understanding, we must observe a source-to-sink system in a forward sense, viewing the processes that create the product. Unfortunately, humans do not have the ability to do this in the natural world due to the time scales involved in source-to-sink sediment transport. Enter experimental geology: Physical experiments, informed by mathematical models, compress time and space, providing ideal conditions to develop a forward understanding of a source-to-sink system. Recent physical experiments have suggested that sediment discharge coming from a source terrane can vary over time, even under constant forcing conditions (Hasbargen and Paola, 2000, Coulthard and Wiel, 2013). If the allogenic forcing on a system is steady, any variations in sediment discharge must be internally generated (autogenic). Under ideal circumstances, autogenic signals may persist through the sediment routing system and be preserved in the rock record where they have the potential to be misinterpreted as changes in allogenic controls.

To date, most experimental studies of autogenic variability have focused on how an environmental signal, created by constant **allogenic** forcing, can be filtered or destroyed by self-organizing processes in fluvial (alluvial) landscapes and subsiding depositional basin, i.e. studies have focused on autogenic processes in the 'sink' terrane. In particular, these studies have focused on autogenic processes that 'filter' allogenic 'signals' from the

source. There has been little work done on autogenic processes in erosional drainage basins, i.e. in 'source' terranes, and how the magnitude of these autogenic signals varies with allogenic forcing (tectonics / climate) and bedrock properties.

In this study, I conducted physical experiments to study autogenic variability in sediment discharge created in source terranes exposed to known allogenic forcing. Specifically, I focused on how allogenic controls and bedrock strength contribute to the magnitude of autogenic variability. A second focus of my study was to determine how autogenic variability manifests itself at the shoreline of a depositional system, i.e. if and how autogenic signals generated in the source appear at the shoreline.

I constructed an experimental apparatus that captures the linkage between a source and a sink terrane. In the source terrane, the three main allogenic controls that contribute to topography and autogenic variability in sediment discharge from the drainage basin can be adjusted. These controls are: 1) rock strength, 2) tectonic uplift, and 3) climate (e.g., Whipple and Tucker, 1999). A total of three experimental runs were conducted. In each run, different combinations of allogenic controls were applied to the source terrane, which, over time, approached a state of dynamic equilibrium. Throughout each run, geomorphology and sediment discharge were observed via photo-imagery and a Lidar scanner. In the sink terrane, i.e. in the net-depositional system, the main allogenic control that can be adjusted is sea-level, though this forcing condition remained constant throughout all experiments. The shoreline of the sink was measured through photo-imagery to determine if autogenic sediment discharge signals from the source could be observed in its progradation rate.

2. BACKGROUND

Surface processes and plate tectonics

Movement and interaction of the Earth's lithospheric plates, i.e. plate tectonics, leads to regions of crustal uplift and subsidence. The combined processes of weathering and erosion attack regions where the crust is ***uplifted*** relative to sea level. Precipitation in these uplifted regions gathers and channelizes to form dendritic drainage networks. The interplay of tectonic uplift, river incision, and hillslope processes creates topographic

relief, which supplies the potential energy necessary to transport eroded sediment downstream towards the drainage-basin outlet. I will refer to these regions of crustal uplift and associated drainage basins as 'source' terranes, as they represent the source of sediment for net-depositional sedimentary basins.

Regions of crustal *subsidence* have the potential to trap sediment produced by erosion in uplifted source terranes. Subsidence of the crust provides space to accumulate sediment, and continual accumulation of sediment—and associated burial and diagenesis—leads to the formation of sedimentary rocks in sedimentary basins. I will refer to these regions of crustal subsidence and sedimentary basin formation as 'sinks.' For the purposes of this study, the sink represents a fluvio-deltaic system. Sediment from the source is routed to the sink, where evidence of processes in the source terrane may be preserved in the stratigraphic architecture, provided these signals can survive 'filtering' in the transport system.

The coupling of source and sink terranes forms linked transport systems. Bedrock erosion in a drainage basin (source) generates the sediment supply to an 'adjacent' sedimentary basin (sink). Variability in the source terrane will affect the geomorphic processes along the linked sediment routing system, including the sediment supply reaching the shoreline of the sedimentary basin. Changes to the sediment supply at the shoreline will cause it to transgress or regress (shift landward or seaward), thus recording the variability. The shoreline is an important and sensitive indicator of sediment supply; changes in shoreline position (transgression/regression) are highly visible features in the rock record (Visher, 1999).

One of the goals of this study is to measure how autogenic variability manifests itself at the shoreline of a depositional sedimentary basin. Autogenic variability of sediment supply from the source terrane is unlikely to be 'felt' (and recorded) instantaneously in the sink. It may take substantial time for a signal to develop in the drainage basin and propagate downstream to the depositional basin. Once the signal is transmitted from the source terrane, it must travel through the terrestrial section of the sediment basin, where it is filtered by fluvial processes, before reaching the shoreline. The signal 'travels' via

localized deposition and erosion, e.g. deposition of sediments in (point) bars or on the floodplain of the fluvial system, that has the effect of 'smearing' the signal emitted from the source terrane. Understanding this complicated filtering process is crucial to understanding the time lag—if any—of shoreline response to autogenic variability in the source terrane.

Concept of dynamic equilibrium:

Assuming the uplift rate and climate (precipitation rate) are steady, on 'long' timescales, the erosion rate within a drainage basin will be set by the uplift rate, i.e. the system will reach an equilibrium state in which the total sediment yield (Q_s) balances the product of uplift rate (U) and drainage basin area (A), i.e. $Q_s = U \cdot A$ (Howard, 1994; Hasbargen and Paola, 2000). To see how this works, consider the thought experiment of Figure 2.1, which shows the approach to dynamic equilibrium of an uplifted drainage basin. At time $t = 0$, the drainage basin is essentially a peneplain and the outlet is approximately at sea level. As the landscape is uplifted, erosional rivers try to grade to sea level. Incision caused by this process steepens channel beds and hillslopes. Erosional processes are slope driven, so as the characteristic slopes increase, so does erosion. Early on, uplift dominates the process as erosion attempts to catch up. Topographic relief grows until the characteristic slopes in the system are large enough to have the erosion rate balance the uplift rate. By time $t = 4$, erosion has caught up to uplift and a dynamic equilibrium has been achieved (Figure 2.1). At equilibrium, the land surface is stationary: mean elevation remains relatively constant. Tectonic uplift continually feeds bedrock to the surface, exposing it to erosion; however, when the erosion rate balances the uplift rate, mean land surface elevation does not change. The concept of dynamic equilibrium applies in the sink as well: In a sedimentary basin at dynamic equilibrium, the sedimentation rate balances the subsidence rate and, locally, the land surface (the sediment-water interface) is stationary.
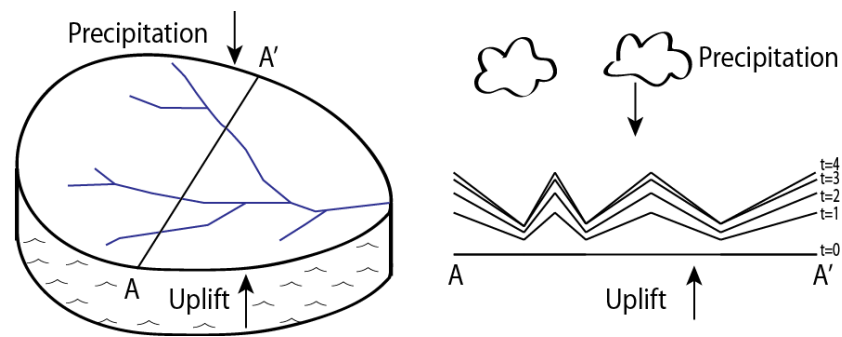
Figure 2.1. Conceptual landscape as it approaches dynamic equilibrium. At time t=0, the landscape is a peneplain. Uplift and precipitation force rivers to incise the landscape, increasing slopes and relief until erosion comes into balance with uplift and time t=4.

How steady is steady-state?

While it makes sense that a source terrane, in both natural and experimental worlds, can—in principle—achieve and maintain a dynamic equilibrium by balancing erosion with uplift, it is unlikely that the sediment discharge (Q_s) exiting a drainage basin will be the steady product of tectonic uplift (U) and area (A). In fact, past physical experiments and numerical models have suggested that there is significant 'noise' (variability) in the sediment discharge signal from drainage basins, even at "steady-state" (Hasbargen and Paola, 2000; Coulthard and Wiel, 2013). In other words, the sediment discharge coming from a drainage basin may fluctuate significantly around a mean value, despite steady allogenic forcing (i.e., steady boundary conditions). Of particular interest, Coulthard and Wiel's (2013) numerical modeling results indicated that autogenic variability of sediment yield can be of the same magnitude as fluctuations caused by external forcing (climate or tectonics).

Autogenic processes in the source terrane

The role of allogenic controls

Sediment mobilization in bedrock drainage basins is caused by multiple factors including earthquakes, precipitation events (storms), underlying geologic structure, and hillslope-channel interactions. Ultimately, fluvial incision into bedrock caused by uplift (or base-level drop) generates relief and causes ridges to become unstable as they approach their threshold slopes, priming them for mass failure events, e.g. landslides. This form of

5

erosion does not take place at a regular rate. Complex interactions between channels and hillslopes cause mass failures to occur episodically (stochastically) and introduce variability into the sediment supply signal transmitted from the drainage basin. In general, the scale of a mass failure is set by the characteristic ridge-relief of the landscape. The scale of relief is set by three main allogenic controls (e.g., Whipple and Tucker, 1999): 1) tectonics (uplift rate), 2) climate (precipitation rate), and 3) substrate (rock strength); the combination of these controls directly influences bedrock incision rates and the scale of mass failures. In the context of this study, it seems reasonable to expect that these allogenic controls set the scale for variability (δQ_s) within the sediment supply signal. Combinations of these allogenic controls that support high ridge relief will, in principle, create the potential for large landslides and high variability within steady-state signals. Alternatively, combinations of allogenic controls that do not support high ridge relief may generate smaller landslides and less potential for variability.

Tectonic uplift at a rate U feeds bedrock to the surface of a landscape, exposing it to surface processes, i.e. channel and hillslope processes. Climate, in the form of precipitation rate (R), sets the available water discharge in the channel network of the erosional drainage basin situated atop the uplifted bedrock. Both of these allogenic variables control fluvial incision and ridge growth. Hasbargen and Paola (2000) combined U and R into a dimensionless variable as a way to compare multiple systems with different allogenic controls. For example, a 'dry' landscape (low R) with muted tectonics (low U) may have similar characteristics as one with a wetter climate (high R) and vigorous tectonics (high U). Landscapes with relatively high U/R values have the potential for ridges with high relief (Whipple and Tucker, 1999; Hasbargen and Paola, 2000; Figure 2.2). If high relief translates to large landslides, then it is possible that a system characterized by relatively large U/R might show greater variability in sediment yield, when compared to a landscape with a low U/R value. This last statement is an overarching idea that will be tested in this study.

Rock strength, i.e. the inverse of 'erodability,' is another variable that contributes to the characteristic ridge relief of a landscape (Figure 2.2). Basins with low rock strength can be easily eroded, leading to ridges with low relief. Alternatively, landscapes with high

rock strength can support ridges that have high relief and steep slopes. Extending the potential correlation between ridge relief, size of landslides, and variability in sediment discharge, it seems plausible that a system with stronger bedrock might display greater variability in Q_s than a system with more erodible (weaker) bedrock. This study also addresses this potential relationship.
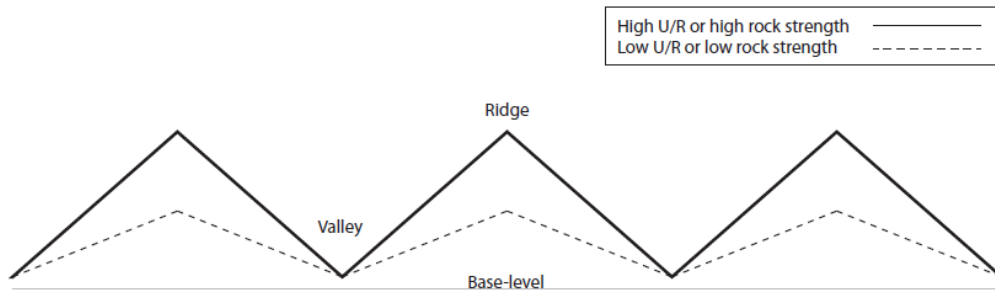
Figure 2.2. Schematic cross section of a hypothetical source terrane landscape with different system parameters. Cross section oriented normal to overall basin slope, i.e. this is a strike section. Landscapes with relatively high *U/R* controls tend to create topography (ridges) dominated by steep slopes and high relief. Likewise, landscapes with high rock strength provide ridges with the mechanical strength necessary to create steep slopes and high ridge relief.

The frequency of autogenic variation

When a mass-failure event (e.g., a landslide) occurs, a sediment volume becomes available for channelized flow to transport from the source terrane. However, evacuation of this sediment volume does not occur instantaneously, so predicting the frequency of autogenic variability in sediment discharge is not as simple as quantifying landslide frequency and volume; in other words, the frequency of landslides in a particular basin does not necessarily set the sediment-variability frequency. Once a mass failure enters a river channel, multiple processes begin to take place. Channelized flow (rivers) in the drainage basin mobilizes landslide-derived sediment piles through a combination of dispersion and translation; dispersion effectively smears out the sediment volume, effectively stretching the duration of the resultant sediment pulse at the basin outlet relative to simple translation. If the landslide volume is sufficiently large, there may be channel damming associated with the landslide. Dammed tributary lakes temporarily store sediment, armoring the channel from further incision, reducing channel slope

upstream of the dam, and inducing deposition associated with a transient backwater effect. These damming processes effectively transmit a 'negative' sediment pulse from the source terrane. In this case, variability may be observed downstream as a period in time when sediment yield is below mean sediment discharge. Ultimately, subsequent flushing of the dam will temporarily increase sediment discharge, creating a pulse of sediment discharge (Capart et al., 2010). One possible effect of dispersion, temporary damming, and the interaction of multiple landslide sediment volumes is to generate an autogenic signal leaving the source terrane that has a periodicity significantly longer than the typical recurrence interval of landslides.

Signal filtering in the depositional system (downstream filtering)
Autogenic processes—bar migration, channel avulsion, delta-lobe switching—in net-depositional fluvial (alluvial) systems typically filter sediment discharge signals that have been transmitted by upland landscapes, regardless of whether they are allogenic or autogenic in nature. Coulthard and Wiel (2013) developed a numerical model that suggests tectonic and climatic changes in a source region create an allogenic sediment discharge signal that weakens with time and distance from the source. Jerolmack and Paola (2010) suggest that autogenic processes in fluvial and depositional systems are due to non-linear behavior in sediment transport. Within a fluvial system, the intermittent behavior of bedload transport and the effects of storage and release of sediment in bars and floodplains can effectively destroy environmental signals, especially high frequency signals.

The extent to which a sediment-supply signal gets filtered (muted or smeared) in the fluvial system depends on multiple factors, particularly the frequency of the input signal (Kim et al., 2006). Fluvial morphodynamics is often treated as a diffusive process, and diffusion tends to act like a 'low pass' filter, i.e. it only passes signals with timescales comparable to or larger than the diffusive timescale of the fluvial system (Paola et al., 1992; Swenson et al., 2000; Swenson, 2005). If changes in sediment supply are relatively rapid, they may not be transmitted to the shoreline. Low-frequency signals, on the other hand, may have the ability to pass through a fluvial landscape, reach the shoreline, and

get preserved in the shallow-marine rock record. The diffusive timescale of the fluvial system varies with the square of the system length, so small systems are less effective at filtering sediment-supply signals. Consider, for example, a natural-world system like Taiwan, where a mountainous source terrane is directly adjacent to a depositional sink. Here, the coastal-plain fluvial system is very short, so its ability to filter a sediment supply signal is minimal (e.g. Liu et al., 2008); conversely, a very large fluvial system, e.g. the lower Mississippi alluvial valley and delta, likely will filter all but the lowest-frequency sediment-supply signals. Finally, the magnitude of the input signal also plays a role in determining whether or not the signal will be preserved. If the perturbation is very large, it is likely that it can pass through the fluvial conduit without being completely destroyed (Jerolmack and Paola, 2010).

A conceptual model of autogenic signal propagation
To conceptualize the propagation of autogenic signals from the source to the sink, consider the cartoons in Figures 2.3a-d. These figure panels represent source-to-sink systems with increasing complexity. Figure 2.3a shows an idealized steady-state devoid of internal (autogenic) variability. Sediment discharge from the source increases rapidly at early times, when uplift dominates the landscape and erosion lags behind, as relief grows. At later times, when ridge relief has grown, erosion balances uplift and the landscape reaches a dynamic equilibrium; once a balance is reached, sediment discharge from the source is constant (steady) in this idealized model. A constant sediment supply to the sink causes the depositional units in the fluvio-deltaic system to have uniform thickness, i.e. the shoreline progrades at a constant rate and the spacing of foreset timelines is uniform (Figure 2.3b).
Figure 2.3c shows what steady-state in the source might look like once autogenic variability is introduced. As in the idealized steady-state model, sediment discharge from the source increases rapidly in small times. The main difference between Figure 2.3a and 2.3c is sediment discharge during large times (when the system is at steady-state). At large times in Figure 2.3c, sediment discharge fluctuates about a mean $\overline{Qs}$, where $\overline{Qs} = UA$, in a cyclic manner. These variations in time are due to hillslope and channel

processes in the source that cause sediments to be eroded in starts and fits. In the sink, variability is preserved in the delta as depositional units with varying thicknesses (Figures 2.3d and 2.3e). The first two depositional packages in the cartoon are the same thickness as in Figure 2.3b. This is done simply to highlight the subsequent changes in package thickness due to autogenic variability. As sediment supply fluctuates through time, the thickness of depositional packages in the sink and the shoreline's progradation rate will respond accordingly. When sediment discharge rises higher than the mean, depositional units in the sink will be thicker than normal and the shoreline's progradation rate will increase. When sediment supply drops below the mean, depositional units will be thinner than normal and the shoreline's progradation rate will decrease. Due to the non-existent fluvial conduit in this model (the source is connected directly to the sink), there is no appreciable time-lag and the two landscapes are in phase with one another.

Figure 2.3c introduces autogenic variability (δQ_s) in the source in the form of fluctuations in the Q_s time series. In this study, autogenic variability is the standard deviation in the Q_s time series; in this figure, autogenic variability can be envisioned as the amplitude of the quasi-sinusoidal fluctuations in Q_s. In Figure 2.3, the potential filtering effects of the fluvial system in the depositional basin are illustrated conceptually by the vertical panel with varying grayscale (shading); a darker shading indicates greater filtering by the fluvial system, which separates the incoming sediment-supply signal (mean and variance) from the shoreline.

Panels 2.3d – 2.3f, conceptualize the possible response of the shoreline for various degrees of signal filtering in the fluvial system. As noted above, multiple filtering processes characterize the fluvial system, including temporary storage in bars and floodplains, channel avulsions, and delta lobe switching; all these processes act as signal filters that can mute, smear, or potentially destroy entirely the sediment discharge variability signals transmitted from the source terrane. In Figure 2.3d, the filtering in the fluvial system is small, and the variability in Q_s from the source terrane is transmitted to the shoreline with very little attenuation: In this scenario, the positive and negative Qs anomalies in time intervals Δt_1 and Δt_2 are passed directly to the shoreline, where they drive enhanced and reduced foreset progradation, respectively. In Figure 2.3e, signal

filtering in the fluvial system is greater, and the direct relationship between variability sediment discharge (δQ_s) and shoreline progradation is more muted and phase shifted. Finally, in Figure 2.3e, filtering is *extreme* and the resultant shoreline response resembles that in Figure 2.3b, i.e. a shoreline prograding in response to variance-free Q_s.
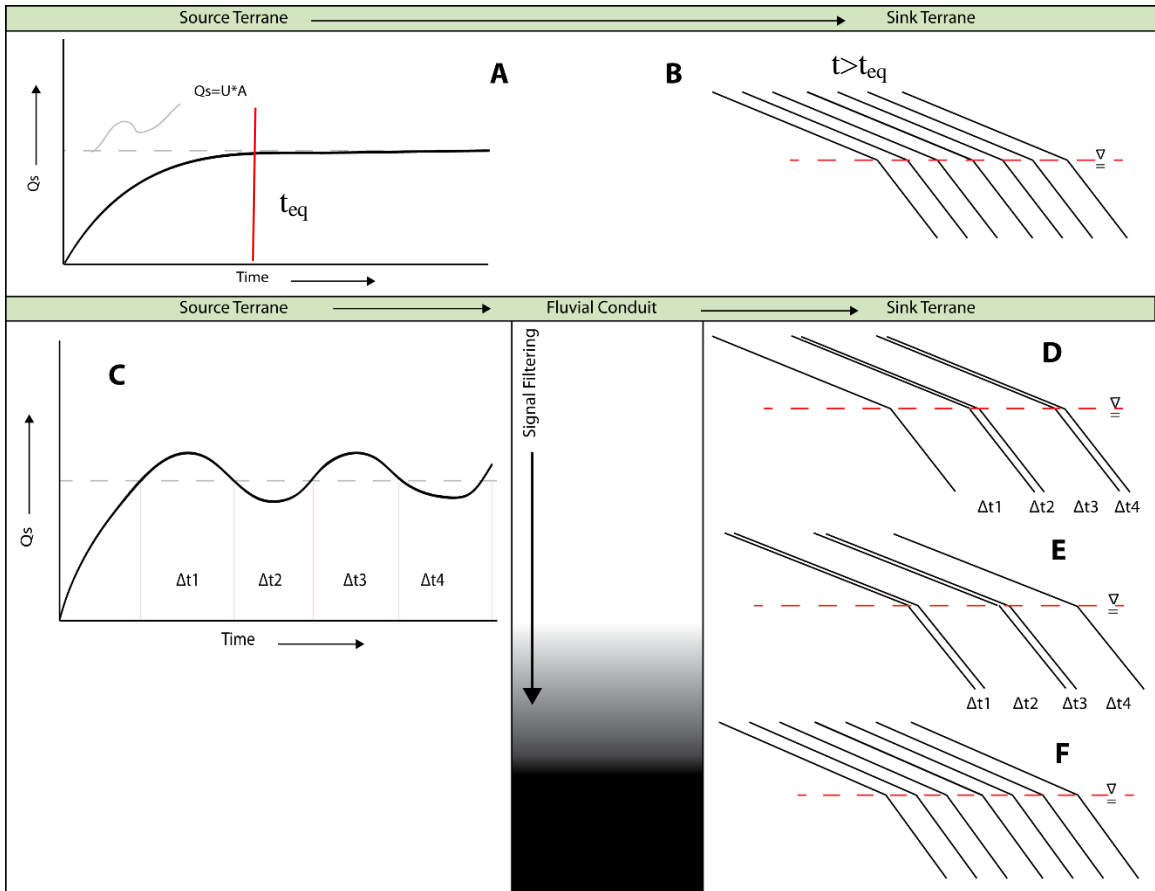
Figure 2.3. Conceptual model of signal propagation in a simplified source-to-sink system consisting of an erosional drainage basin linked to a simple, prograding fluvio-deltaic system. (A) Approach to dynamic equilibrium in source terrane without autogenic processes, i.e. with no internal variability in sediment discharge. (B) Cross section showing shoreface progradation in response to steady sediment yield from equilibrated source terrane in (A). (C) Sediment yield from source terrane with autogenic variability. (D-F) Shoreface progradation in response to 'noisy' sediment supply from (D) with varying degrees of filtering in the fluvial system: (E) little if any filtering of sediment-yield variability; (F) significant filtering of variability in sediment yield. Refer to text for details.

11

Why laboratory scale experiments?

Field-based studies of signal preservation in stratigraphic architecture are complicated and filled with uncertainty. Paola et al. (1996) and Paola (2000) provide excellent summaries of the challenges of field-based stratigraphic studies. While sedimentary rocks preserve information about allogenic and autogenic controls during their deposition, later tectonic uplift and erosion are required to exhume these deeply buried sedimentary rocks and allow us to study them directly. This erosion and uplift likely removed a considerable volume of rocks and, using the same reasoning, a considerable volume of the preserved signal we want to study. Also, in contrast to igneous rocks, sedimentary rocks are very difficult to date numerically. As a result, it is very challenging to establish age relationships and process rates in ancient sedimentary sequences.

These 'operational' issues pose major problems, but a bigger complication to field-based study involves the very nature of stratigraphy and stratigraphic studies. In a *forward* sense, physical *processes* in the source and sink terranes lead to the formation of a *product*—the sedimentary rocks. Studying sedimentary rocks directly is an *inverse* problem: We only have the *product*, from which we try to say something about the processes that formed it. For example, to establish a link between autogenic processes in the source terrane and shoreline migration in the sink, we need corresponding evidence in both end-members of the sediment routing system, i.e. evidence in the drainage basin and in the sedimentary basin. But source terranes are the erosional sections of the system. Their erosional nature makes it (largely) impossible to preserve historic signals—the information has been obliterated. Therefore, we cannot directly associate preserved shoreline movements in the sink with processes in the source because no history of autogenic or allogenic processes exists in the source terrane. In practice, in most 'deep time' stratigraphic studies, there is no direct evidence of the source terrane—only the sink remains.

Mathematical models (theory) can provide insight into how signals are passed from the source to sink (Tucker and Hancock, 2010; Paola, 2000). The main problem with mathematical models is that we do not know how to represent mathematically the physical processes at work, particularly on geologic timescales.

One way around some of the issues of field-based and theoretical studies is to use carefully designed laboratory experiments. These physical experiments of landscape evolution and sedimentation allow us to see how the natural world functions on short timescales; by 'reducing' the natural world into a laboratory setting, we can view the evolution of a landscape in mere hours or days. Not only do physical experiments shrink space and time, they also allow us to control external forces that are applied to the system. We have complete control of climate, tectonics, and bedrock lithology. Basically, we can run a forward (physical) model—with complete control of the system inputs—and generate experimental stratigraphy; we can then dissect this stratigraphy and associate—with confidence—process and product.

The use of physical experiments to study erosional (e.g., Schumm et al., 1987; Hasbargen and Paola, 2000) and depositional (Paola et al., 1996; Postma, 2008) processes has increased significantly over the past two decades. My research builds on the experimental work of Leslie Hasbargen and the research group at Saint Anthony Falls Laboratory; much of this experimental work was conceived and supervised by Professor Chris Paola (UMTC). Hasbargen created a physical model of an uplifting, eroding drainage basin with the purpose of providing a physical test for numerical landscape evolution models (Hasbargen and Paola, 2000). In his experiment, he forced steady rainfall and uplift rates onto a tank of sediment while monitoring the behavior of the drainage network that developed. Paola et al. constructed the Experimental Earthscape Facility (a.k.a. 'Jurassic Tank'), a large subsiding basin designed to test theory of sedimentation on continental margins (e.g., Paola, 2000). My work couples an uplifted erosional drainage basin to a subsiding sedimentary basin, thus forming the first (to my knowledge) source-to-sink experiment.

Laboratory scale experiments on landscape evolution and sedimentation are not without shortcomings. As noted by Paola et al. (2009), the biggest issue is that of 'scaling.' A laboratory-scale drainage basin is not simply a 'scaled down' version of a natural drainage basin. Classical scaling techniques—such as those used in open-channel hydraulics—do not work. However, a laboratory-scale drainage basin has a tributary network of erosional channels coupled to hillslope processes; the channels and hillslopes

erode the substrate ('bedrock') in a way that generates channel networks and behavior grossly (and statistically) similar to their natural-scale cousins. The same basic ideas hold true for experimental sedimentary basins (e.g., Paola, 2000). The main point here is that we can gain physical *insight* from these small-scale systems, even if the underlying physics does not scale precisely.

3. PROBLEM STATEMENT

This study addresses the magnitude of autogenic variability in the net-erosional drainage basin and the relative importance of allogenic forcing (tectonics and climate) and rock strength in controlling this variability in sediment discharge (Q_s) from the drainage basin. In addition, this study attempts to assess the extent to which autogenic signals generated in the net-erosional drainage basin are recorded in the sedimentary record of the linked depositional basin.

With respect to autogenic variability in the net-erosional experimental drainage basin, the null hypothesis (H_o) is: *The magnitude of fluctuations in sediment discharge (δQ_s) from the source terrane is independent of uplift rate, precipitation rate, or rock strength.* Formally, the alternative hypotheses (H_1 and H_2) are tied to the idea that uplift/climate and rock strength control topographic relief and thus the magnitude of sediment-discharge variability:

H_1: *Increasing uplift rate (U) and/or decreasing precipitation (R)—as embodied in the dimensionless number (U/R)—generate an increase in variability (δQ_s).*

H_2: *Increasing 'rock' strength—as embodied in clay content—generates an increase in variability (δQ_s).*

In the experimental sedimentary basin, variability in the rate of shoreline progradation serves as the measure of preservation of autogenic signals that originate in the coupled drainage basin. Hence, for this problem, the null hypothesis (H_o) takes the form: *Fluctuations in shoreline progradation rate are uncorrelated with fluctuations in sediment discharge*. A strong alternative hypothesis (H_3) has the form:

H_3: Fluctuations in shoreline progradation rate are correlated with fluctuations in sediment discharge and the shoreline response is lagged relative to δQ_s.

The experiments performed in this study were designed to benchmark the newly-constructed apparatus and test the above hypotheses.

4. METHODOLOGY

Experimental Apparatus

I designed and constructed an experimental apparatus with the ability to trace sediment transport from source to sink. This apparatus represents two distinct experimental landscapes that have been physically linked (Figures 4.1-4.3). The first landscape is a net-erosional drainage basin that simulates a tectonically-uplifted source terrane. The three allogenic controls that contribute to a landscape's characteristic topography—rock strength, tectonic uplift rate, and climate—are all represented in the experimental source terrane. The combination of uplift and precipitation causes a drainage network to form in the erosional source terrain. Laboratory-scale valleys and ridges are created as the basin organizes itself to evacuate water and sediment. As channels incise the landscape, surface water and eroded sediment travel downstream to the second experimental landscape, a net-depositional sedimentary basin that simulates a sink terrane. The sedimentary basin provides a body of water for source-supplied sediment to be deposited into a fluvio-deltaic environment. Increasing the elevation of the free surface in this basin mimics a rise in relative sea level. Changes in relative sea level, which represent the sum of (tectonic) subsidence and fluctuations in eustatic (global) sea level, create the necessary space for preservation of the sedimentary rock record.

Figure 4.1. Source to sink experimental apparatus. The source terrane (left side of the image) is located in a stainless steel drum. PVC misters are located directly above the source terrane. Shower curtains are used to contain water and funnel it into a drain located below the source. The sink terrane (right side of the image) is essentially a plastic flume with metal supports to maintain its structure. Note the delta and 'sea level' inside the flume. Sea level is set by a weir found at the far end of the flume. An aluminum structure encases the entire apparatus. On top of the structure is a track system, on which a motorized cart carrying a Lidar scanner is utilized. The scanner has the ability to measure surface topography of both the source and sink terranes.

Figure 4.2. A view from the far end of the sink terrane (sedimentary basin), looking towards the source terrane (drainage basin). Sediment and water exit through the slot running vertically down the center of the source terrane as a metal dam is slowly lowered (simulating base level fall/tectonic uplift). All sediment and water travel down a stainless

steel ramp that physically connects the two basins. Steel supports on top of the depositional flume provide support and keep the flume's walls from bowing.

A. Side View

B. Top View
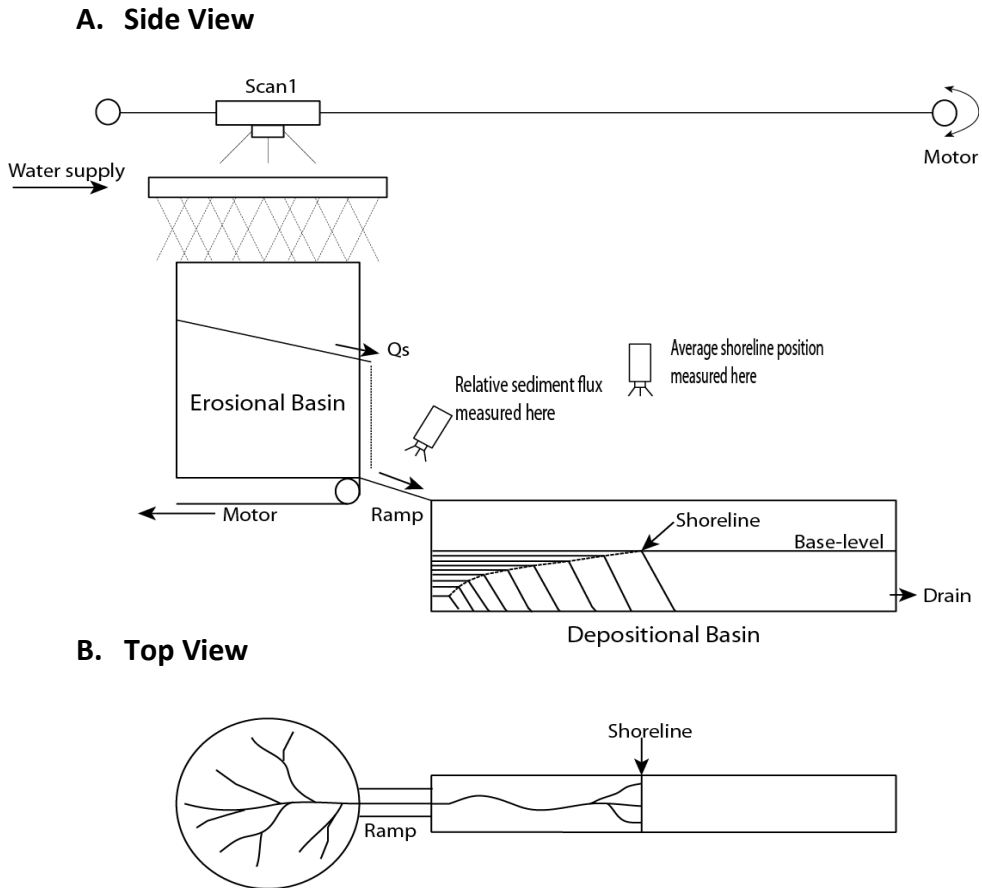
Figure 4.3. A schematic drawing of the experimental apparatus. The upper drawing (A) is a side-view and the lower drawing is a map-view. Water enters the apparatus through a series of hoses, valves and PVC pipes that have been fitted with misters. A motor located beneath the source terrane (erosional/drainage basin) slowly lowers a metal dam, allowing sediment and water to exit the drainage basin. Sediment and water travels down a ramp on its way to the sink terrane (depositional basin). A weir and drain system allows sea-level to be adjusted and set over a range of 'elevations'. A Lidar scanner has the ability to measure the surface topography of both basins. Relative sediment flux can be measured at the ramp by a camera, though this process is still being worked out and, at the time of this study, not utilized. A camera above the depositional basin measures shoreline position through time.

The Source Terrane:

Design:

The erosional source terrain apparatus was designed to emulate key attributes of
Hasbargen's experimental drainage basin (Hasbargen and Paola, 2000). It consists of a
stainless steel tank, 95 cm tall and 80 cm in diameter, filled with a mixture of silica sand
and a small amount of kaolinite; the clay provides 'cohesive strength' to the granular
mixture. On the side of the tank is a 5cm-wide slot that extends nearly its entire height. A
strip of stainless steel dams the slot, holding all of the sediment inside the tank. The
uppermost end of the strip, known as the gate, sets base level for the erosional drainage
basin; any sediment above this elevation is "free" to leave the basin, while everything
below it is held in place by the strip. The other end of the strip is connected to a step-
motor-controlled Velmex Bi-slide housed beneath the tank. The stepped motor slowly
pulls the strip downward at a controlled rate, effectively dropping the gate and base-level
and thereby mimicking tectonic uplift.

Figure 4.4. A view inside the drainage basin. Both images were taken by a GoPro camera
during Run 2. The terranes slope towards the outlet located on the right side of both
images. Note the slot on the right side. A stainless steel dam sets base level at the
slot/outlet.

Rock Strength:

A mixture of sand and clay is used to create the sediment packages used in each experiment. Sand provides the bulk of the sediment mass (all experimental runs contained between 95 and 98% sand). Clay provides the necessary cohesion for the source landscape to develop ridges. Because of this, it acts as a proxy for rock strength in this experiment. As the clay concentration increases, so does the 'rock' strength. This has a profound impact on the topography and overall behavior of a landscape. Stronger rocks allows for steeper and taller ridges, which, in turn, generate larger landslides.

In the experimental runs analyzed here, the median grain size (D_{50}) of the sand was 100 microns. With the range of precipitation rates used in the experiments, this sand was mobilized as bedload in both the erosional and depositional basins. In contrast, the clay particles were transported entirely as washload and, as such, did not affect the morphodynamics of channels.

Tectonic uplift:

The step-motor allows the user to control the rate at which base-level drops. This process is equivalent to uplifting the landscape relative to base-level. In other words, if the motor is programmed to drop base-level at a rate of 1 cm/hour, it is effectively simulating tectonic uplift of the entire source landscape at that same rate. As uplift is applied to the basin, a drainage network develops and rivers incise the landscape as they attempt to grade to base-level. A wide range of uplift rates can be programmed into the motor; however, for a given rock strength and climate, determining a reasonable uplift rate that yields physically reasonable drainage networks is not at all trivial and consumed a significant amount of time.

Climate (precipitation):

A misting apparatus, attached to a water supply through a garden hose, is fixed 50 cm above the top of the tank. This apparatus provides relatively uniform precipitation over the landscape. The misting apparatus consists of two square PVC rings, stacked on top of one another and fitted with grocery store "vegetable misters." The upper misting ring is fitted with hollow-cone misting nozzles and the lower ring is fitted with full-cone nozzles. Full-cone nozzles permit a higher discharge rate than the hollow cone nozzles.

Three different misting configurations and, therefore, three discrete precipitation rates are possible: When the lower misting ring is open, the precipitation rate it 7 μm/s. The upper ring provides a slightly higher precipitation rate of 9 μm/s. Opening both rings at the same time provides a precipitation rate of 16 μm/s. Precipitation rates can be fine-tuned through a gate-valve located at the garden hose/misting ring junction. There is also a pressure gauge located at this junction, which provides a measurement of the water pressure entering the misting rings. Through a series of dedicated experiments, precipitation rates were calibrated to account for different water pressure values at each of the three misting configurations. Further, a pressure vs precipitation curve has been created for each configuration. With this curve for reference, precipitation can be fine-tuned by adjusting the gate-valve until a desired pressure is reached.

The Sink Terrane:

The second experimental apparatus is designed to represent a net-depositional sink environment, i.e. a sedimentary basin. It is a rectangular, acrylic tank 30 cm wide, 60 cm tall, and 2.5m long. The narrow dimensions of this basin were chosen to allow sediments to aggrade and prograde rapidly and to encourage the formation of a channelized fluvial environment in the proximal part of the basin. Water and sediment from the erosional basin pass over a stainless steel chute that physically connects the two basins. The chute is 15 cm wide with 5 cm tall sidewalls, which is sufficiently large to prevent deposition. The chute link connects the two basins and, in a natural setting, would represent a zone of sediment bypassing between net-erosional and net-depositional terranes.

An adjustable weir located at the distal part of the depositional basin sets base level. Water flowing over the weir enters a reservoir where a pump removes it from the system. By setting base level to a constant value (e.g., 5cm), the depositional system is forced to be progradation-dominated. In principle, during steady-state in the erosional system, sediment discharge is constant and the shoreline's progradation rate is steady, though it does slow in time as the delta topset grows and more sediment can be stored in it. Changes in sediment supply from the source basin—be they allogenic or autogenic in origin—thus trigger periods of transience in the depositional basin, causing its shoreline

progradation rate to change accordingly. This process is captured in a photographic time series.

Figure 4.5. Side view of the depositional basin during Run 2. A delta has formed on the left side of the flume, where sediment and water from the drainage basin enters. A camera and a light source sit directly above the flume and record shoreline position through time. A weir on the far end of the flume sets sea-level and creates a reservoir on the right side of it. A pump drains the reservoir, sending water to the same drain that empties the source terrane.

Experimental design:

The overarching hypothesis for this experiment is that *autogenic* variability scales with characteristic relief of a landscape, which in turn depends on uplift rate, precipitation rate, and rock strength (clay content). *Allogenic* forcing that causes systems to have relatively high relief will, in turn, create the potential for high autogenic variability in sediment yield signals. Systems with relatively small mass failures create a more continuous and consistent supply of eroded sediment than systems with large mass failures and will, therefore, have less variability in their sediment yield signals. This hypothesis was tested by measuring variability in steady-state sediment discharge from source terranes exposed to multiple combinations of allogenic forcing, i.e. tectonic uplift, precipitation, and rock strength.

Three experimental runs were performed for this study. Each of these three runs had a unique clay concentration (i.e. rock strength). Climate and tectonic uplift, the two other allogenic controls, were varied during each the three experiments. These two controls are

21

represented by the dimensionless variable *U*/*R*, where, again, *U* is uplift rate and *R* is precipitation rate. This dimensionless variable is useful in this study because it combines climate and tectonics into one variable, allowing us to isolate the effects of rock strength more easily. Table 1 summarizes the parameters used in each experimental run.

Run	Clay (% by weight)	Uplift (*U*) (μm/s)	Precipitation (*R*) (μm /s)	*U*/*R*	Run Time (hrs)	Scan Interval (hrs)
1	2	3.2	24	0.13	0-20	2.00
			17	0.19	20-40	
2	5	3.2	17	0.19	0-13	0.50
		9.6		0.56	13-22.5	
		4.8		0.28	22.5-26.5	
3	4	3.2	17	0.19	0-17.5	0.50
		9.6		0.56	17.5-21	0.33

Table 4.1. Parameters used in all three experimental runs. Clay content simulates rock strength. Uplift is simulated through base-level fall at the drainage basin outlet, which is controlled by a stepper motor located below the basin. Uplift rates are controlled through a computer program. Precipitation rates are set by a series of valves that sets the amount of water allowed to flow through PVC pipes above the drainage basin. U/R is a dimensionless variable used to characterize controls forced on the drainage basin.

Another goal of this study was to assess the potential for autogenic fluctuations in sediment yield from the source terrane to be 'preserved' in the depositional system. In the context of the current experimental configuration, this exercise amounted to recording variations in the shoreline progradation rate and attempting to correlate those with variations with sediment yield.

Measurements:

The two key observables in this experiment are sediment supply leaving the drainage basin and migration of the shoreline. These observables are measured through the use of digital elevation models (DEMs), ArcMap GIS, and photographic images.

Imaging in the source terrane:

The surface topography of the erosional basin is measured by a Faro 3D LIDAR Scanner. The scanner, which provides digital elevation maps (DEMs) at millimeter-scale precision, operates on an automated cart and measures the topography from a fixed position squarely above the erosional basin (Fig. 4.3). LIDAR scanning occurred on a regular schedule that is determined by the allogenic conditions forced on the source terrain in each individual experiment (See Table 1). For each DEM, ArcMap is used to determine the volume of sediment in the source tank (using a fixed bottom, a fixed outer perimeter, and the surface topography as boundaries). The volumetric difference between consecutive DEMs is then calculated, providing a volume of sediment eroded from the tank between scans. By dividing this volume by the amount of time that passed between scans, a sediment discharge rate (Q_s) is calculated. This method of discharge calculation is effective for obtaining highly-accurate, long-term discharge rates from the drainage basin. Its limitation lies in the averaging that occurs when discharge is calculated over long time periods, i.e. it provides a low-resolution view of discharge and 'misses out' on individual events, e.g. individual landslides, that take place within a scanning interval. For each run, periods of 'steady-state' were determined based on the value of $\frac{Qs\ observed}{Qs\ theoretical}$ for every scan, where Q_s *observed* is the volumetric difference between DEMs divided by time between scans. At steady-state, Q_s *theoretical = UA*, where *U =* uplift rate and *A =* basin area. When multiple (more than 5) consecutive scans had values close to unity, the system was determined to be near steady-state. Q_s *theoretical* also provides a steady discharge from which a standard deviation from the mean can be measured. In this study, standard deviation is the proxy for autogenic variability in Q_s. Other data are extracted from the DEMs as well, including local and regional relief (DEMs combined with Geographic Information System software offers a powerful tool in landscape analysis; however, this thesis focuses on relief and volumetric differences over time so many of the ArcMap tools will not be discussed further). Local relief is measured by using the topographic profile tool in ArcMap. For each DEM, two topographic profiles across representative ridges are measured and exported into Excel, where relief

on both sides of the ridge is averaged to determine a characteristic ridge-relief for the landscape. Regional relief for each DEM is determined by finding the difference between the topographic high and low points over the entire landscape. This topographic characteristic provides insight into the size of potential mass failures and the regional slope of the landscape, which is an important factor in understanding the ability of a landscape to evacuate sediment. A landscape with a relatively low slope may not be able to evacuate a mass failure as quickly as one with a relatively high slope. This has implications for the ability to transmit or filter a sediment-discharge signal.

GoPro imagery provides a tool for short-term measurement of individual landsliding events and their subsequent evacuation from the source terrane. A GoPro Hero 4 camera is set up above the source terrane and programmed to take a photo every minute. The ability to view the source terrane at one minute intervals allows for 'unzipping' the data obtained through DEM analysis; it provides much finer detail of the events that take place throughout the experiment. These photos can be imported into time-lapse programs to view landscape evolution and individual events in 'real time'. Landslide counts were performed for each uplift rate during Run 2, the most successful of the three runs. By using GoPro imagery, one can count and measure the landslides that were averaged/filtered out during DEM analysis and determine how long it takes a given landscape to disperse landslides. Information gathered from these images is used to understand the processes that create autogenic variability within the sediment supply signal.

Imaging in the sink terrane

Measuring shoreline movement is relatively straightforward. Shoreline position is documented through a series of digital photos taken every minute from above the depositional basin using a Canon DSLR camera. Measuring tape is located just above sea-level in the depositional basin, providing spatial reference when observing the shoreline in each image. Viewed from above, the shoreline position may be irregular across the width of the basin (Figure 4.6). Measurements are taken at the left side, right side, and center of the shoreline to determine average shoreline position for each photo.

Shoreline position paired with time stamps from each photo provide the variables needed to calculate instantaneous shoreline progradation rates.

A small, 'artificial' delta is constructed at the head of the depositional basin to accelerate the delta-building process. The addition of this artificial delta allows shoreline measurement to take place at 6.5 hours into the experiment instead of the 12+ hours it takes without one (based on data gathered in the first two runs). The delta is constructed out of sand and allowed to grow after construction for several hours to allow self-forming processes to shape it. Once it looks natural and has extended out from the 'splash zone' at the head of the basin by at least 20 cm, shoreline measurement can begin. During Run 3, the delta is reset to its initial length at the start of high uplift.

Sediment discharge rates and shoreline progradation rates are tested for correlation through the Pearson product-moment correlation coefficient. For consistency shoreline progradation rates are averaged over DEM scanning interval for the given run. Doing so smooths the shoreline data and creates a shoreline 'match point' for every sediment-discharge (Q_s) data point obtained from the source terrane.

Figure 4.6. Image of fluvio-deltaic shoreline in experimental system. Topset of sandy delta is located towards the top of the image; the angle-of-repose delta foreset extends seaward of the shoreline, beneath the milky-colored free surface. Milky color of the 'ocean' is a result of suspended clay. Measuring tape stretched out directly above sea-level, on the inside of the flume walls provide spatial reference. Due to channel migration

25

and the construction of 'lobe like' features, the shoreline plan-view shape changed regularly; hence, average shoreline position was calculated by measuring position on both edges and in the center of the flume. Crater-like features on topset the result of water droplets.

5. RESULTS AND DISCUSSION

I conducted three experimental runs in this study, each with different combinations of rock strength, tectonic uplift, and climate (precipitation). The three runs had varying levels of success, but they all contributed significant value to this thesis and towards future applications of this experimental apparatus by exploring how it works and responds to multiple combinations of parameters. Run 1 demonstrated that the source terrane has the ability to come to dynamic equilibrium under constant forcing conditions, which is an important foundation for the theories and hypotheses within this thesis. Run 2 improved on Run 1 by utilizing a newly formed sediment mixing method to create a homogenous sediment package. It also included smaller Lidar measurement windows to provide a higher resolution of sediment discharge from the basin. Finally, Run 2 improved on Run 1 by introducing GoPro imagery, which provided one-minute snapshots of the basin, further increasing resolution and allowing us to witness individual events. Run 3 successfully connected the source to the sink, allowing us to observe a unique sediment supply signal in both terranes. Prior to the third run, mechanical problems in the sink limited confidence in shoreline data.

The following section will present the results for all three runs. In the interest of brevity I will combine experimental results and the ensuing discussion into a single section. Specifically, I will describe the parameters that contributed to the behavior of each run as well as the geomorphic processes that resulted from them. I will also discuss the variability of sediment discharge for each combination of parameters. Variability, in the context of this thesis, will be presented multiple ways. First, variability will be presented as the raw standard deviation in Q_s at dynamic equilibrium. Second, variability is presented as the standard deviation in Q_s normalized to the mean observed sediment discharge rate at dynamic equilibrium. Lastly, variability is presented as the standard deviation in Q_s normalized to the theoretical sediment discharge rate at dynamic

26

equilibrium. In the latter two scenarios, when variability in sediment discharge (δQ_s) is normalized with some value of Q_s the normalized variability will be presented as a simple percentage, i.e. ($\delta Q_s / Q_s$) · 100.

Run 1:

Parameters:

Experimental Run #1 was conducted over 40 hours and designed to test the effects of two *U/R* conditions by varying precipitation midway through the experiment. The bedrock substrate represented low rock strength. At 2% clay by weight, this run had the weakest rock strength of the three experimental runs. Uplift remained at a constant 3.2 μm/s throughout the experiment, while precipitation changed halfway through. For the first half (20 hours) of the experiment, a relatively high precipitation rate of 24μm/s was used, creating a U/R condition of 0.13. A reduction in precipitation to 17μm/s occurred at *t* = 20 hours, increasing the U/R condition to 0.19 (Table 5.1).

Lidar scans were taken every 2 hours through the entirety of the experiment. The long time intervals between scans filtered out much of the short-term variability occurring in the source terrane, resulting in relatively low temporal-resolution data of sediment discharge at the basin's outlet. Scans were taken every 2 hours in this run because I was unaware of how the system would behave and because I was using a separate tool, a "fluxometer", to sample sediment discharge at the source outlet every 10 seconds. The fluxometer, had it worked properly, would have provided an extremely high-resolution measurement of sediment variability over the course of the experiment. Unfortunately, the fluxometer data were inconclusive, and the only measure of sediment discharge from this experiment was the Lidar scans taken every 2 hours.

Even though Q_s data coming out of the source terrane were relatively low resolution, they provided evidence that this experimental apparatus does, in fact, work and that the source landscape will reach dynamic equilibrium, if given enough time to do so. These results helped to guide later runs and gave an idea of the amount of time it takes a landscape in this apparatus to reach dynamic equilibrium, i.e. the 'response time' of the erosional

source terrane. This first experimental run also gave insight into how much variability we could expect to see in Q_s data.

Geomorphic Processes:

The approach of the drainage basin to topographic steady-state is displayed in Figures 5.1. Initially, i.e. at time $t = 0$, the basin is a peneplain. Over the course of 20 hours, the landscape is dissected by headward eroding channel knickpoints propagating upstream from the basin outlet. At the time of full-dissection, there were approximately 5-7 ridges in the drainage basin with an average relief of about 1.3 cm (Table 5.1). In comparison to the ridges measured throughout the three experimental runs, these ridges have the *least* amount of relief. The channels between the ridges are also wider than the channels in other runs (Figures 5.1, 5.3). These features are best explained by the high precipitation rate used in the first half of this run (i.e. by a low U/R value) and by the relatively low rock strength. In the context of the dimensionless number U/R, this system could be described as 'precipitation dominated,' i.e. U/R is relatively small. Precipitation dominated the landscape, causing small-scale mass failures along ridges and easily transporting eroded sediment downstream through wide, alluvial valleys that resembled braided channel networks. This precipitation dominance also caused a relatively low basin-wide slope of 0.23 (measured from the outlet of the basin to the furthest upstream boundary). While this slope seems very large compared to natural-world conditions, it is near the minimum of basin-wide slopes measured in this study. In laboratory scale experiments, river slopes are typically several orders of magnitude larger than their natural counterparts (e.g., Sheets et al., 2002; Paola et al., 2009). Because channels did not need to concentrate water into incised channels in order to evacuate sediment from the landscape, there was minimal incision in the wide, alluvial valleys of this landscape. At 20 hours into the experiment, the precipitation rate was lowered by approximately 30%. Effects of precipitation change were noticeable in ridge relief. By reducing water discharge in the landscape, rivers needed to concentrate themselves into narrow channels. Narrowing caused incision and allowed ridges to increase in relief and width. Average

ridge relief increased by 0.8 cm to 2.1 cm. Basin-wide relief also increased by 1 cm, causing the average slope to increase to 0.24.
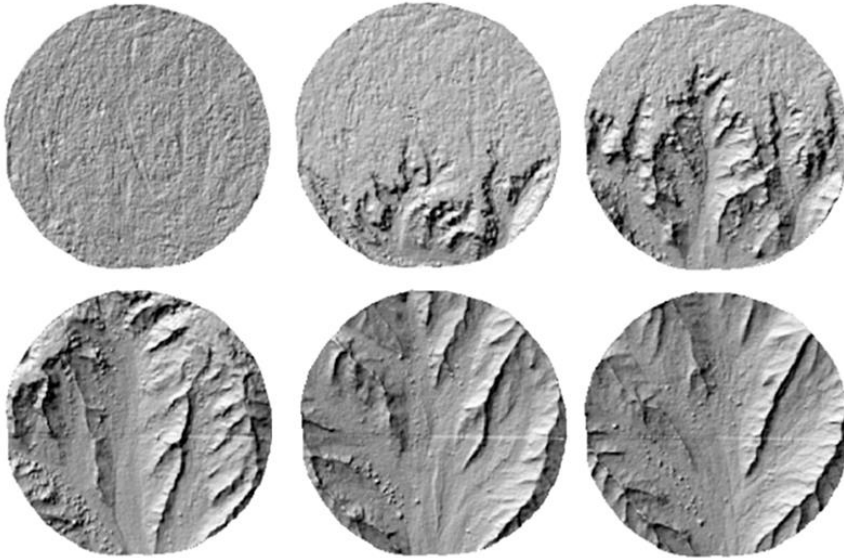

Figure 5.1. Approach to dynamic equilibrium as reflected in the source-terrane topography of experimental Run 1. Upper left panel shows initial peneplained surface; lower right panel shows fully dissected system near equilibrium. Temporal spacing of images is 4 hours.

Sediment Discharge:

Figure 5.2 shows sediment discharge (Q_s) at the drainage basin outlet. During the initial landscape dissection phase, sediment discharge increases steadily. The landscape comes to steady-state approximately 15-20 hours into the run, when Q_s data in Figure 5.2 stabilize (at about 84% the theoretical mean). For the remainder of the experiment, sediment discharge fluctuates about the theoretical steady-state value of Q_s from Equation 1 (i.e., $Q_s = U{\cdot}A$).

Overall, variability in sediment discharge was relatively low throughout Run 1 when compared to the other runs. Low variability is most likely due to a combination of factors. A low uplift rate (U) combined with low rock strength creates conditions where ridges cannot sustain high relief. Low relief results in relatively small mass failures along the ridges. High rates of precipitation relative to uplift create high carrying capacities in river channels, allowing them to quickly evacuate landslides from the drainage basin. The

long period of time between Lidar scans also contributes to the lack of variability by smoothing out sediment discharge data over two hour windows.
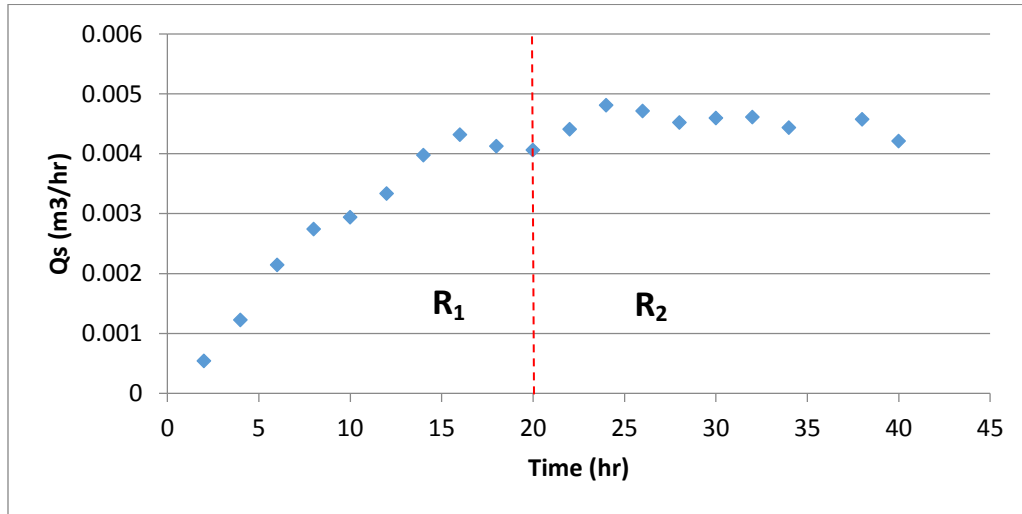

Figure 5.2. Time series of sediment discharge (Q_s) from the drainage basin for experimental Run 1. Precipitation was reduced at $t = 20$ hours.

All three measures of variability in Q_s increased when precipitation rate was reduced from 24 μm/s to 17 μm/s (Table 5.2). A reduction in precipitation rate (the 'climate' proxy) lowers the ability to erode ridges efficiently, allowing uplift to be more important than it was during the high-precipitation phase of the experimental run. The precipitation reduction also narrows river channels which, in turn, widens ridges and allows them to grow. Larger ridges (relief and width) have the potential to host large mass failures which likely contribute to higher variability.

Both phases (high and low precipitation) of this run included long periods of time where the drainage basin was close to steady-state. During high precipitation, the observed sediment discharge was 84% of the theoretical mean. During low precipitation, observed discharge was 94% of the theoretical mean. With the basin near steady-state during both of these phases, it is interesting to observe a significant difference in normalized variability, i.e. 3.0% vs. 4.7%. Because uplift was steady throughout the experiment, the theoretical sediment yield coming out of the basin should not change. This suggests that the observed increase in variability was caused primarily by a reduction in precipitation.

In other words, the drainage basin has the same theoretical mean sediment yield at both climates, yet variability increases when precipitation is reduced. This observation suggests strongly that climate change alone can cause sediment-yield variability to change with it, i.e. changes in climate alone can generate non-trivial changes in autogenic variability in sediment supply. This observation is consistent with the numerical model of Coulthard and Wiel (2013), which suggested that climate-change signals are more likely to be seen in sediment supply yield than are tectonic-change signals.

Run	U/R	Rock strength (clay as a %)	Mean ridge relief (m)	Mean basin slope (%)	Observed mean Q_s (m^3/hr)	Standard deviation (m^3/hr)	Standard deviation normalized to observed Q_s (%)	Standard deviation normalized to theoretical Q_s (%)
1	0.13	2	0.013	0.23	4.12E-03	1.47E-04	3.56	3.0
	0.19	2	0.021	0.24	4.65E-03	2.33E-04	5.01	4.7
2	0.19	5	0.042	0.33	2.33E-03	5.61E-04	24.1	12.0
	0.56	5	0.075	0.43	1.15E-02	1.60E-03	14.0	11.3
	0.28	5	0.072	0.40	9.03E-03	8.43E-04	9.34	12.0
3	0.19	4	0.017	0.21	3.48E-03	2.49E-04	7.16	4.7
3	0.56	4	0.020	0.29	1.21E-02	9.42E-04	7.81	6.0

Table 5.1. Summary of measured (observed) variability in sediment discharge and other parameters from the drainage basin for the three experimental runs. The second column contains the ratio of uplift to precipitation rates (*U/R*), which changed within each experimental run.

Run 2:

Experimental Run 2 was the most successful of the three in this study in terms of physical appearance of the landscape and the quality of GoPro and Lidar imagery. It is because of these factors that Run 2 will be the main focus of this Results and Discussion section.

Parameters:

Run 2 used a substrate of high rock strength and variable tectonic uplift rates to investigate their respective influences on variability. At 5% clay, Run 2 had the highest rock strength of the three experiments (Table 5.1). Three uplift rates were used through the experiment while precipitation rate (*R*) was kept at a constant 17μm/s. Approximately

55 cm of sediment was exhumed throughout the run, which lasted a total of 26.5 hours. For the first 13 hours of the experiment, a relatively low uplift rate (U) of 3.2 μm/s was used. From hours 13-22.5, uplift rate was tripled to 9.6 μm/s. For the remainder of the experiment (hours 22.5-26.5), uplift was adjusted to 4.8 μm/s. Lidar scans were taken every 30 minutes to increase the resolution of sediment discharge data relative to Run 1. While this reduced sampling interval was an improvement, it could not capture single events (e.g., mass failures and their subsequent evacuation from the drainage basin). Instead, it time averaged the events that took place within a 30 minute period (instead of the 2 hour period seen in Run 1). To observe events, a high-resolution, waterproof GoPro camera was installed above the source terrane and programmed to take a photo every 60 seconds.

Low uplift rate, 0-13 hours:

Geomorphic Processes:

During initial dissection of the peneplained initial drainage basin (U=3.2 um/s; U/R = 0.19), five prominent ridges developed as four 'interior channel' knickpoints propagated upstream from the basin outlet (Figure 5.3); these interior channels have self-formed ridges on either side, as opposed to channels that formed along the outer boundary of the basin. Compared to Runs 1 and 3, ridges in Run 2 were relatively wide and the channels were relatively narrow. Average ridge relief during the first 13 hours of the experiment was approximately 4 cm (Table 5.2) and the basin-wide slope of the terrane was approximately 0.33%.

During the low-uplift phase of Run 2, the drainage basin organized itself to erode efficiently the high-strength bedrock. This characteristic organization included five ridges, four main channels, and a relatively high basin-wide slope (Figure 5.3). Uplift rate and, as a result, sediment discharge were low enough such that relatively small channels could evacuate sediment efficiently.

Landslides are the dominant erosional mechanism in the experimental drainage basin; simple reasoning suggests that their frequency of occurrence and characteristic volume (size) likely are important controls on the autogenic variability in sediment supply (δQ_s).

The following simple analysis provides a framework for interpreting observations of landslides in the experimental system.

For a given uplift rate, precipitation rate, and rock strength, if landslides have a *characteristic* volume V [L^3], then the time-averaged sediment discharge from the basin Q_s [L^3/T] is

$$Q_s = fV \tag{1}$$

where f [1/T] is the frequency of landslides. This relation has two degrees of freedom, i.e. the system can adjust either frequency (f) or volume (V) of landslides. At dynamic equilibrium:

$$Q_s = fV = UA \tag{2}$$

where, as previously defined, U [L/T] and A [L^2] are the uplift rate and area of the drainage basin, respectively.

Landscape volume (V) is difficult to quantify directly via measurement in the experimental system. However, we can measure landside frequency (f) with relatively high confidence, provided the events are sufficiently large to image with available cameras. With frequency known (observed), simple rearrangement of Equation 2 gives:

$$V = \frac{Q_s}{f} = \frac{UA}{f} \tag{3}$$

Hence, if the system is near dynamic equilibrium, we might expect landslide volume to scale like U/f, i.e. higher uplift rates and lower landslide frequency both generate larger volume landslides. In the experiments, f is simply the number of observed landslides (N) per time interval (T), something we measure with high-frequency GoPro imaging. While the frequency of landslides (f) can be measured in a relatively straightforward manner, thereby providing a measure of landslide volume, the meaning of 'high' or 'low' frequency is less than clear. Presumably, the meaning of high frequency is a function of the intrinsic rates that characterize the physical system; for an erosional drainage basin, the erosion rate would seem a logical measure of process rate. The concept of 'fast' and 'slow' in the erosional drainage basin requires a timescale; one possible choice for a timescale (τ) is the characteristic relief in the system (Z) divided by the uplift rate (U), which itself sets the scale for the basin-scale erosion rate:

$$\tau = \frac{Z}{U} \tag{4}$$

Equation 4 simply represents the effective 'residence time' for a parcel of bedrock (experimental substrate) experiencing surface erosion represented by the network of hillslopes and channels with characteristic relief Z. Equation 4 is roughly analogous to the 'scouring time' of Sheets et al. (2002), which characterized the time interval a fluvial channel is exposed to reworking in a subsiding, net-depositional sedimentary basin. We can construct dimensionless (or scaled) landslide frequencies (φ) using this timescale:

$$\varphi = f\tau = \frac{N}{T}\frac{Z}{U} \tag{5}$$

Assuming the time interval (T) of landside counting does not vary between observations, the dimensionless frequency of landsliding scales like NZ/U, i.e. for a count (N), a system with high relief and/or low uplift rate will have a relatively large dimensionless frequency. Stated alternatively, for a measured landslide frequency f [1/T], a drainage network with a larger erosional residence time τ will have a larger scaled landslide frequency. The effect of a large residence time—a 'slow' system, from an erosional perspective—is to stretch the frequency, thereby making landslides *appear* more frequent.

Landslide frequency during this low-uplift-rate phase of the experiment was measured through the use of GoPro imagery. During a 30 minute interval, when the system was nearest to steady-state, there were approximately 65 landslides (Table 5.2, Figure 5.3). These landslides were small (typically 2 cm x 2 cm) in area and volume (Table 5.2), as the failure rarely extended more than halfway up the height of a ridge. Landslides were dispersed relatively quickly by rivers and were barely recognizable as sediment slumps within minutes of the initial failure, i.e. the slumps lost their visual coherence within minutes (Figure 5.4).Channels were never dammed by landslides in this portion of the run, *sensu* Capart et al. (2010), as rivers had the capacity to disperse quickly slugs of sediment. Note that dimensionless frequency of landsliding was relatively large during this low-uplift phase (Table 5.2). In other words, in a scaled sense, the channel-hillslope interactions were such that landsliding was frequent.

Uplift phase	Uplift rate (μm/s)	Relief (m)	Landslide count (N)	Frequency (f; min^{-1})	Residence time (τ; min)	Volume (V; cm^3)	Frequency (φ; [0])
Low	3.2	0.042	65	2.17	219	45	474
High	9.6	0.075	83	2.77	130	105	360
Inter.	4.8	0.072	47	1.57	250	92	392

Table 5.2. Characteristics landslide attributes during the three phases of Run 2. Final two columns represent landslide volume (V) and dimensionless (scaled) frequency (φ).
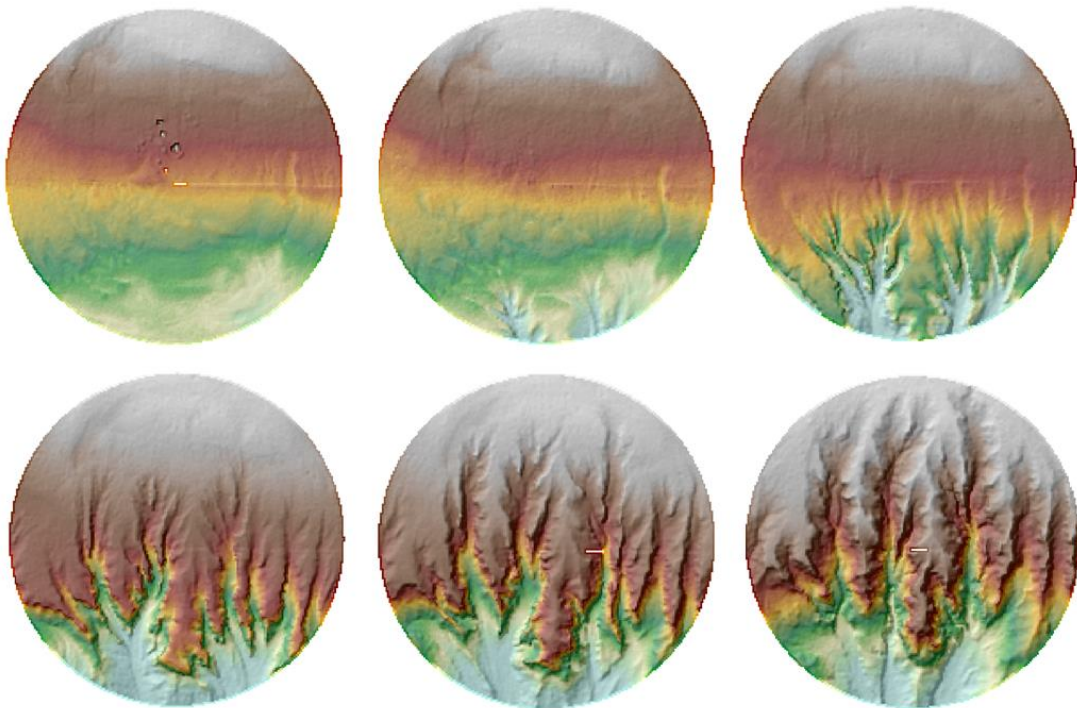

Figure 5.3. Approach to dynamic equilibrium as reflected in the source-terrane topography of experimental Run 2 at relatively low uplift rate. Upper left panel shows initial (approximately) peneplained surface; lower right panel shows fully dissected system near equilibrium. Temporal spacing of images is 150 minutes. Compare with Figure 5.l.
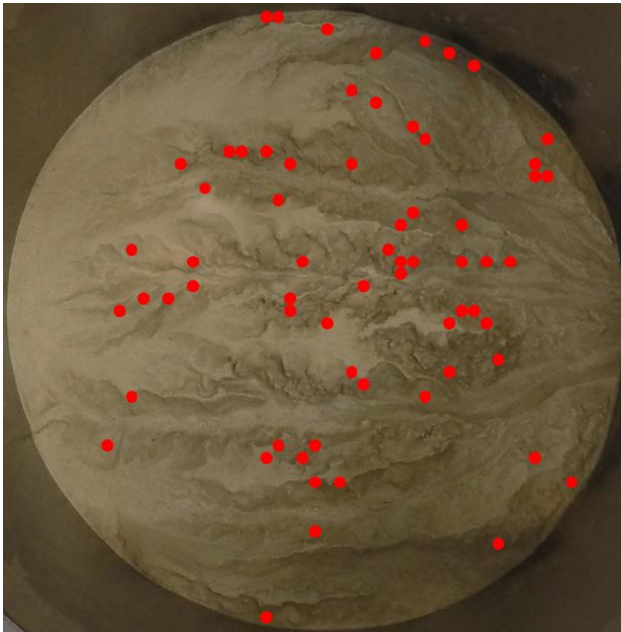
Figure 5.4. Locations of landslides during a 30-minute sampling interval in Run 2 under conditions of low uplift rate. A total of 66 detectable landslides were observed in the interval. Landslides were distributed fairly uniformly over the surface of the drainage basin.
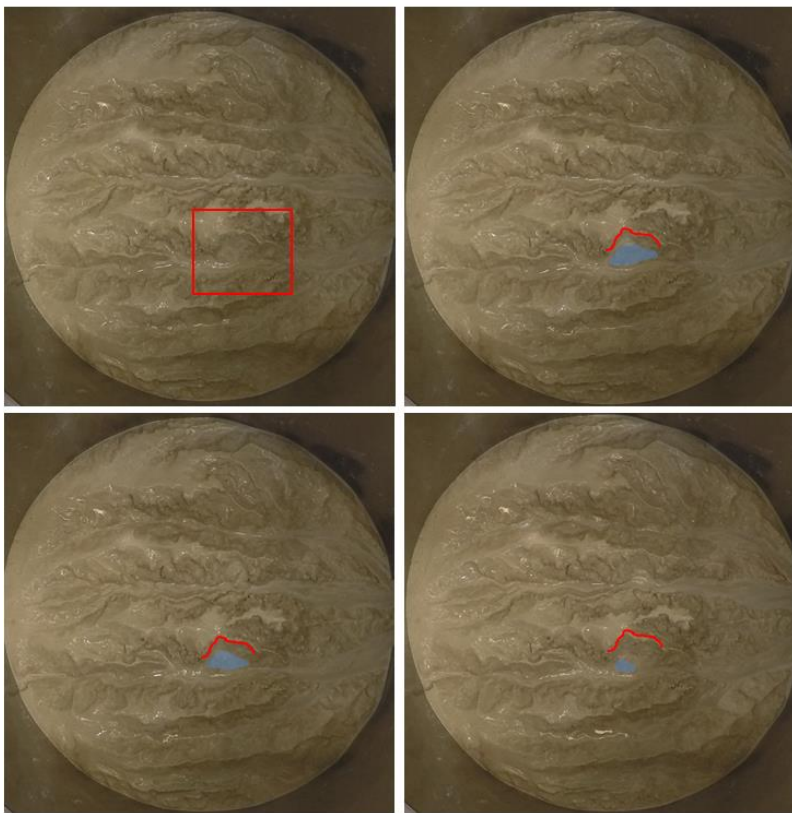

Figure 5.5. Landslide sequence under low-uplift conditions. Upper left panel shows location of landslide, which is bounded by the red curve. The slumped material is denoted by the blue shading. Over the course of 5 minutes, landslide is almost completely dispersed by fluvial processes.

The Q_s time series in Figure 2.6 shows how sediment discharge gradually increases over the first 13 hours of the experiment. At early times (0-8 hours), the majority of sediment discharge can be attributed to the headward erosion of channel knickpoints migrating upstream as the initial peneplain condition is dissected and the basin attempts to reach an appropriate overall slope. Very few landslides occur along the sides of ridges during initial dissection; however, as the ridges continue to grow, the likelihood of mass failures increases, especially closest to the outlet where uplift is most impactful. These factors contribute to the relatively low variability seen in the early portion of the run. During hours 8-13, variability in Q_s appears to increase. This is likely due to the fact that a large percentage of the basin is dissected and ridge relief has reached a level conducive for relatively large mass failures in the lower reaches of the basin. Over the course of 13 hours, sediment discharge had an uplift-normalized variability of approximately 11% (Table 2).
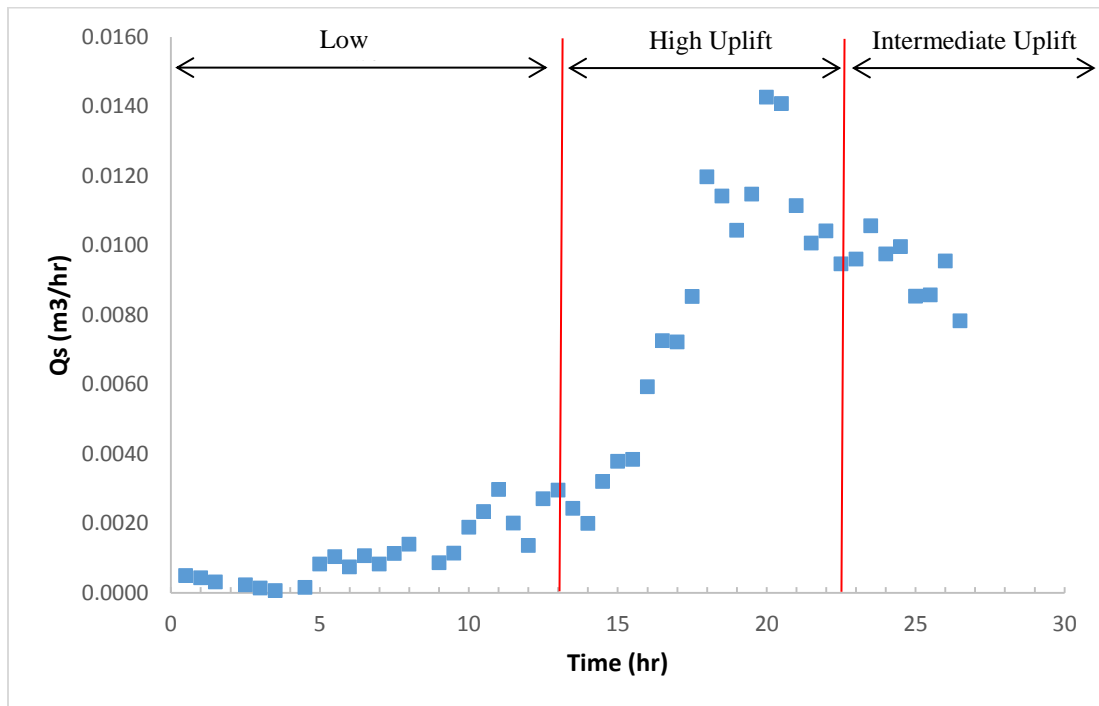

Figure 5.6. Time series of sediment discharge (Q_s) for Run 2. Changes in tectonic uplift rate occurred at $t = 13$ hours and $t = 22.5$ hours. Data obtained from differencing Lidar images at 30 minute intervals.

High uplift rate, 13-22.5 hours

Geomorphic Processes:

At t = 13 hours, when tectonic uplift rate was tripled, the source terrane needed to re-organize itself to deal with this significant change in allogenic forcing. Channels began to incise almost immediately, causing all five ridges to grow in relief, width, and length (Figure 5.7). Incision was so pronounced that at times features resembling ravines occurred in channels mid-way between the basin outlet and divide (cylinder wall). Ridges grew to an average relief of 7.5 cm, causing the size of landslides to increase with time. Large mass failures throughout the basin caused temporary channel blockages (tributary damming, *sensu* Capart et al. 2010), and knickpoints continually migrated upstream as the basin attempted to find an appropriate representative (overall) slope to deal with the sudden increase in uplift rate. Approximately 3 hours into high-uplift phase, a massive shift in basin organization became apparent. The two ridges that flank the center ridge were cannibalized. Deep incision caused ridge relief to grow quickly and ridge slopes to become unstable. The ravine features that were created by deep incision behaved as knickpoints, initially occurring near the middle of the basin and eventually moving to the upstream portion of the basin, i.e. near the bounding cylinder wall. With the wave of deep incision propagating upstream, came an increase in mass failure magnitude and frequency that eventually consumed the two ridges by eroding their sides (Figure 2.8). Channel knickpoints also contributed to the destruction of these ridges by constantly attacking their front, or nose.
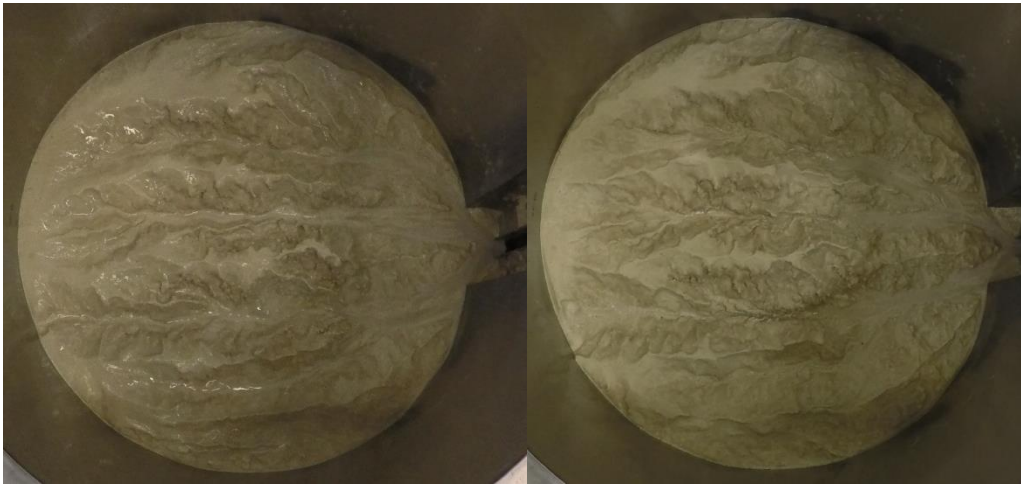
Figure 5.7. Images of the basin immediately before uplift was increased (photo on the left) and one hour after (photo on the right). Tripling uplift caused the ridges to grow in length, width, and relief. These changes are most noticeable near the outlet of the basin (right side of each photo) where knickpoints originate. Note the incision along the lower face of the center ridge in the 'after' photo. Steep, narrow ravines were commonly observed migrating upstream throughout this portion of the run.
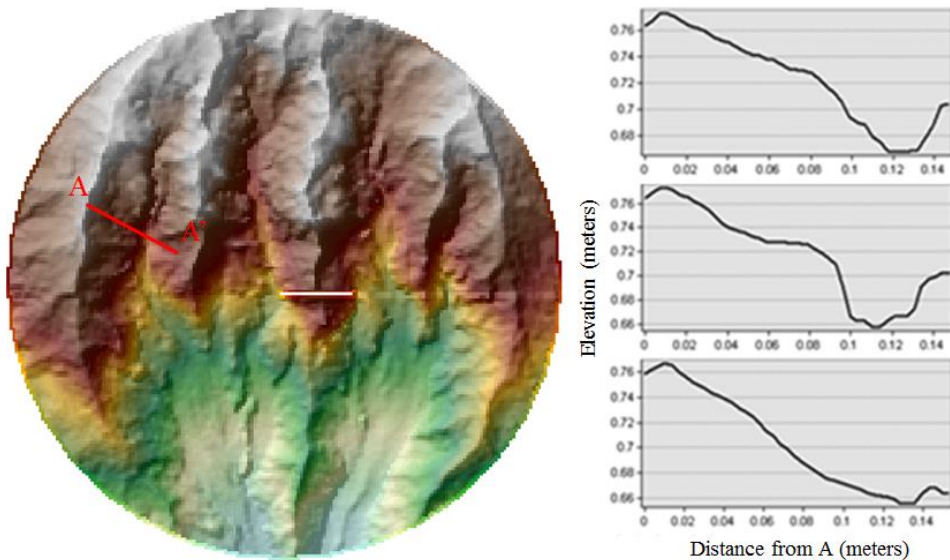
Figure 5.8. Composite imagery showing how a large landslide occurs across a ridge over the course of two hours as the second ridge from the left is cannibalized during basin re-organization. The topographic profiles on the right show how sediment was evacuated across profile A-A'. The upper profile was created immediately after a wave of channel incision reached the region of the profile and the banks of both ridges begin to steepen. The center profile shows highly steepened slopes on both ridges as incision continues. Eventually the slopes fail, creating large landslides that are evacuated by the river

39

(bottom profile). This process provides large sediment slugs to river channels, while temporarily stabilizing hillslopes until future waves of incision reach the area.

In response to the increased uplift rate, it was necessary for the basin to re-organize itself into fewer ridges and channels. By tripling uplift rate, theoretical (equilibrium) sediment discharge from the basin was also tripled. Because there was no corresponding increase in precipitation available to help channels the additional sediment load, the basin needed to concentrate all of its surface water into two main channels that were capable of transporting sediment downstream (Fig. 5.9). These channels had an average basin-wide slope of 0.42, an increase of about 10% from the low-uplift phase. This large-scale re-organization of the drainage network was associated with a major increase in sediment discharge, as reflected in the Q_s time series of Figure 5.6, which shows a major transient response beginning at 13 hours of run time. Eventually, the basin approached steady-state and the main driver of erosion (and, therefore, sediment discharge) transitioned from basin-wide re-organization (five ridges to three) to individual landslides.
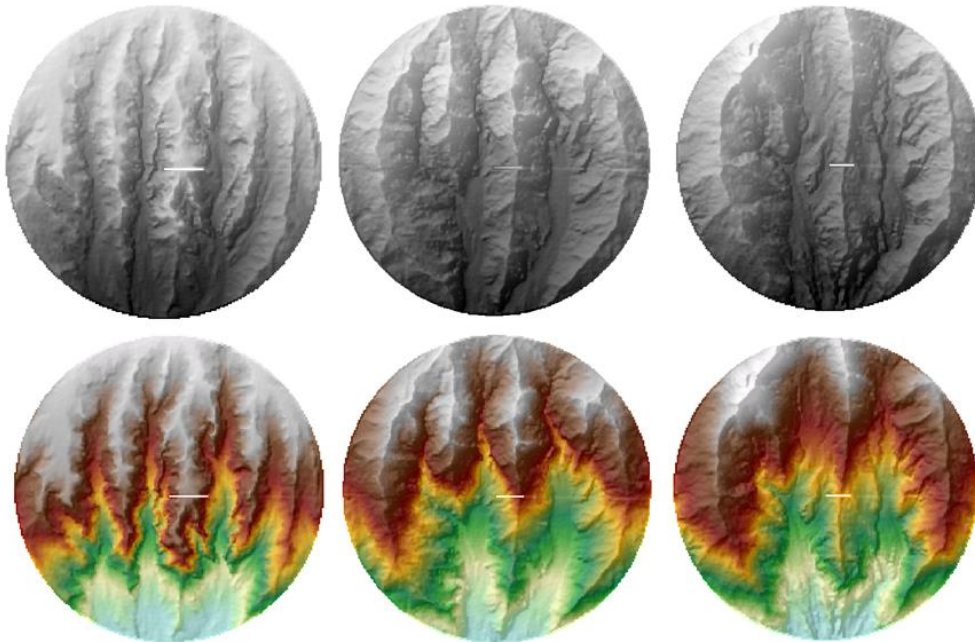

Figure 5.9. Drainage-basin response to three-fold increase in uplift rate showing large-scale, long-term basin re-organization. The upper row of DEM images show re-organization over 4 hour time intervals. Greyscale was used to highlight the features of

each ridge. Not that as two of the ridges are cannibalized (ridges two and four when counting from the left), the remaining ridges get larger. Drainage density decreases as the basin re-organizes itself, presumably to enable an increase in sediment discharge to be evacuated from the basin. The lower row of DEMs represent the same times as the upper row but are shown in color to get a better sense of the topographic character through time.

At steady-state, large landslides continued to occur on the three main ridges. Some of these landslides were so large that a single event had multiple impacts throughout the valley in which it occurred. Mainly, these mass failures caused channel blockages, or damming events, which required substantial time intervals for removal. Sediment slugs of this size often persisted for tens of minutes at the channel reworked itself in order to adjust to the new conditions (Figure 5.10). While the river channels eventually dispersed all landslides, the system usually took a relatively long period of time to do so, and the course of the river was typically altered. Figure 5.10 also shows how a large landslide can create a chain of events that ultimately causes large amounts of sediment to be eroded from the landscape in long, high amplitude pulses. As a mass failure occurs on the north-face of the southernmost ridge, its sediment creates a large blockage in the river channel. Because the channel lacks sufficient competency, it was forced to travel around the landslide, changing its course to one that butted it up against the south face of the center ridge. The channel also needed to decrease its width in order to start dispersing the sediment pile. The combination of these events created an incised channel along the edge of the center ridge, which, in turn, led to a large mass failure on its south face. This chain of events propagated downstream in a coherent 'wave-like' pattern that resembled—in effect—a 'reverse' mass-failure knickpoint.
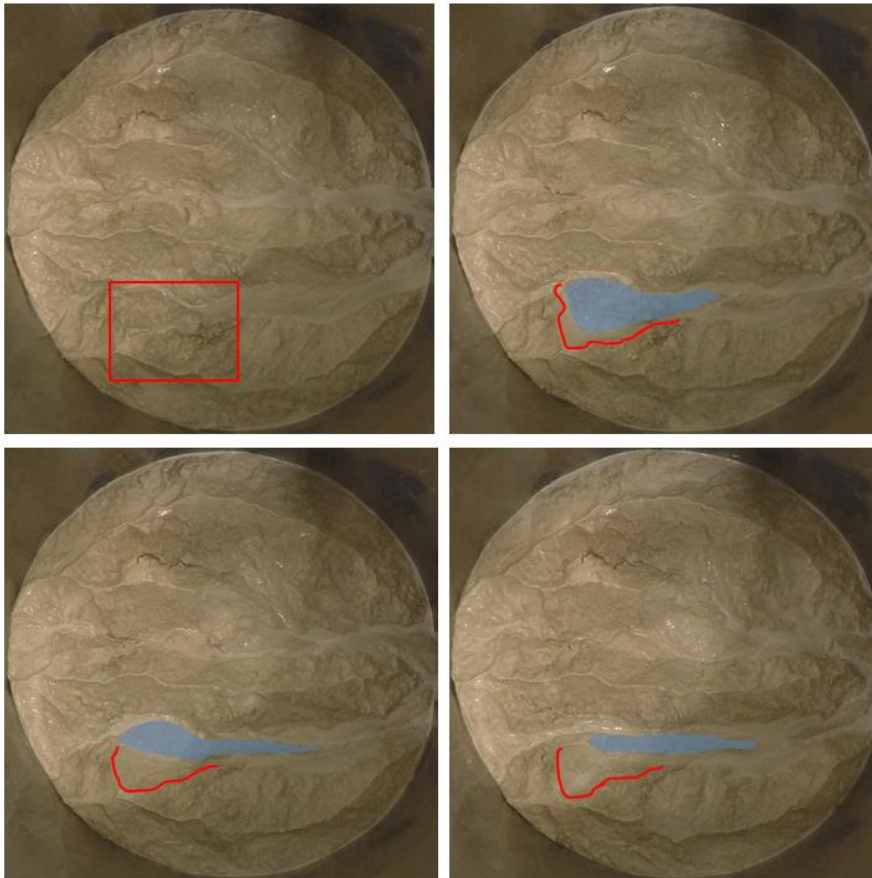
Figure 5.10. Landscape response to a representative landslide in the high-uplift rate phase of Run 2. Upper left panel shows the location of the landslide; lower right panel shows the extent of reworking after 20 minutes. Panel spacing is five minutes. Note how the landslide forces the channel up against the south face of the center ridge, causing another landslide. While the second landslide event is not highlighted in this figure, it can be inferred based on the thinning of the center ridge.

Landslides were much larger—by nearly a factor of two (Table 5.2)—during the high-uplift rate phase of the experiment and—when measured with respect to actual time—occurred more frequently (Table 5.2). In total, there were 83 landslides observed over a representative 30 minute period, when the system was near dynamic equilibrium (Figure 5.11). Given the increased relief that resulted from a higher uplift rate, we might expect the size of landslides to increase accordingly. What is less obvious is the relationship between landslide frequency (rate of occurrence) and uplift rate. In a dimensioned sense, the frequency of landslide increased by approximately 35% in this high-uplift phase of

the experiment. However, when viewed through a non-dimensional lens, the frequency of landsliding actually decreased (Table 5.2). Stated alternatively, when measured relative to the residence time of bedrock exposed at the surface, i.e. τ, the recurrence interval ($1/f$) of landslides increased, thereby resulting in a decrease in scaled frequency (φ).

Figure 5.11. Landslide count at high uplift (83 in 30 minutes); red dots denote locations of landslides, which are distributed relatively uniformly along the lengths of ridges.

Intermediate Uplift

At 22.5 hours into the experiment, uplift was reduced to 4.8 μm/s. This intermediate uplift rate continued for the remainder of the experiment (a total of 4 hours). A lack of available sediment in the drainage basin limited the duration of this final portion of the run. The decision was made to reduce uplift rate to this intermediate value in order to explore how the drainage basin would respond to different combinations of parameters and to observe the geomorphic processes that unfolded when uplift is decreased, rather than increased.

Geomorphic Processes

By reducing uplift, ridge relief was forced to decrease with time. At the end of the four hours dedicated to intermediate uplift rate, ridge relief had decreased slightly, from an average of 7.5 cm to 7.2 cm, and the basin-average slope decreased from 0.42 to 0.40. Characteristic ridge relief was achieved through two main geomorphic processes. First, large mass failures continued to develop throughout the basin; characteristic landslide volume only decreased by about 10% (Table 5.2). Some of these slides were as big as or even bigger than those during the high uplift phase. These large failures may reflect a lag in the system, i.e. the basin was still 'feeling' the effects of the high uplift phase. This seems to be the case in the uppermost ridge where, during the latter stages of high uplift, a series of deeply incised "ravines" formed. These ravines likely destabilized a face of the ridge; the subsequent large landslides occurred despite the reduced uplift rate, not because of it. The other explanation for these large landslides is that erosion was adjusting to tectonics as the basin approached a new steady-state, thus causing the ridges that were developed during high uplift to have multiple failures as they shed their excess relief.

The second process that reduced characteristic ridge relief occurred in the two main channels. Large landslides deposited their sediments into the channels and, as the rivers dispersed and translated these sediments, their beds appeared to *aggrade* with time. The combination of large landslides and a reduced uplift rate caused the river channels to fill in with sediment, leading to significantly wider, alluvial channels that are in contrast to the incised 'bedrock' channels seen during high uplift.

 The drainage basin had insufficient time to reach a steady-state at the intermediate uplift rate. Average sediment discharge during this portion of the run was approximately 1.25 times the theoretical steady-state discharge rate for an uplift rate of 4.8 μm/s. During this transient phase, in which the basin-wide erosion rate was decreasing from its high-uplift-rate value, sediment discharge from the source terrane was driven by large landslides and alluvial processes that reworked sediment slugs through dispersion and translation. Excess sediment from large mass failures (possibly a relic of the high-uplift phase) often clogged river channels. It seemed to take a longer time to disperse sediment slugs from

large landslides during this intermediate-uplift phase; they often persisted for tens of minutes and sometimes accreted onto downstream sections of a ridge, effectively creating new land by widening the ridge at that point in the basin.

During this intermediate-uplift-rate phase of Run 2, a total of 47 landslides occurred during a representative 30 minute period, e.g. Figure 5.12, a considerably lower dimensioned frequency than either of the previous phases of this run (Table 5.2). In a non-dimensional sense, the scaled frequency of landslides increased slightly. The frequency-magnitude data for this phase of the experiment should be interpreted with caution because the system had not reached dynamic equilibrium when counting statistics were measured. Nonetheless, the characteristic landslide volume (V) and dimensionless frequency (φ) are consistent in that they assume intermediate values relative to the high- and low-uplift phases.

Figure 5.12: Landslide count at intermediate uplift rate (47 landslides). Light blue arrows point to 'ravine-like' features that formed during this phase of landscape response.

Run 2 Sediment discharge:

Variability in sediment discharge, in the form of raw standard deviation, increases with uplift throughout this run. When normalized to *observed* sediment discharge, however, variability behaved differently. For example, variability in sediment discharge during low uplift was 24.1 %, compared to 14.0% and 9.3% during high and intermediate uplift, respectively. This is most likely due to the fact that the source terrane never fully reached steady-state. Sediment yield from the drainage basin was still increasing during the initial transient phase. Therefore, the mean sediment discharge used when calculating this form of variability was artificially low, causing variability in this method to be erroneously high.

When normalized to incorporate the equilibrium sediment discharge for a given uplift rate, variability remains relatively constant (11.3-12.0%). In other words, variability, as a percentage of steady-state discharge, appears to have changed relatively little with uplift rate. However, the observed frequency and magnitude of mass failures that drive variability did change significantly. Further, the ability of a river channel to evacuate a mass failure changed as well. Ultimately, the sediment discharge and variability values in Table 2 only tell part of the story of sediment-yield signals from the source. The data in Table 5.1 cannot explain how sediment supply signals from the basin actually look at a smaller temporal scale. Is sediment transmitted through high-frequency/low amplitude pulses, through low-frequency/high amplitude pulses, or through some other combination? The data of Table 5.2 provide some insight into the this smaller-scale behavior. In addition, high-frequency GoPro imagery allowed for analysis of ridge-channel interactions and mass failure evolution in nearly real-time, lending insight into how single events contribute to sediment supply variability exiting the source terrane. An analog for how landslides are evacuated from the source is shown in Figure 5.13, where the main trunk of the river channel exiting the source terrane is represented by a conveyor belt that delivers sediment to the net-depositional sink in pulses, the amplitude and frequency of which depend on the volumes and frequencies of landslides as well as the capacity of channelized flow to evacuate sediment. Conceptually, small, frequent landslides create low amplitude, high frequency signals that are unlikely to persist

46

through a fluvial conduit to the shoreline. Large, relatively infrequent landslides create high amplitude, low frequency signals that may persist through a fluvial conduit and be preserved at the shoreline.
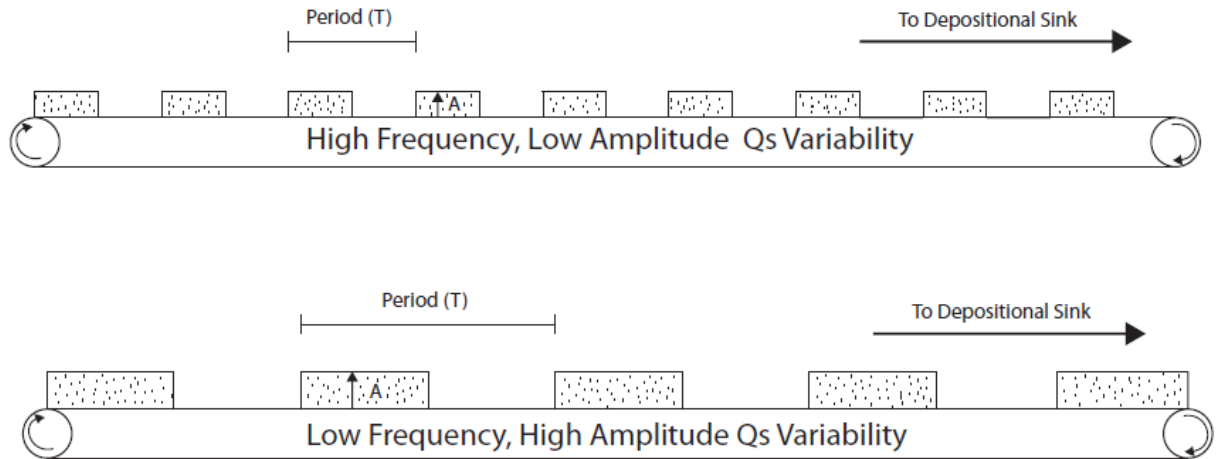

Figure 5.13. Conveyor-belt analogy showing how the interplay of landslide frequency and volume with the sediment-carrying capacity of channels generates autogenic variability in the sediment supply to the depositional sink. The meaning of period (*T*) depends on the process timescales of the source and sink systems.

The amplitude and frequency of individual landslides may not correlate directly to the amplitude and frequency of the sediment supply signal. Based on detailed analysis of high-frequency GoPro images, it seems that the interaction of landslide slumps with the channelized flow may be the deciding factor as to what a sediment-signal looks like. A single, large mass-failure event may take tens of minutes for the river to disperse and evacuate downstream. This 'reworking' timescale is an order of magnitude larger than the periodicity of landslides (~minute), thus giving rise to complex interaction between multiple landslides. In effect, channels must rework multiple landslide slumps simultaneously, unlike low-uplift (low-relief) systems, where small landslides are reworked rapidly and in relative isolation. The net effect seems to be a stretching effect that causes sediment supply pulses to persist for relatively long periods of time, perhaps allowing for long, coherent autogenic signals at the basin outlet. As Jerolmack and Paola

(2010) point out, it is such low frequency signals that tend to survive the 'shredding' in the fluvial system and thus be preserved in the rock record.

Run 3:

Parameters:

At 4% clay by weight, this run represented intermediate 'rock' strength. Throughout the run, precipitation was kept constant at 17 μm/s. Uplift was set to 3.2 μm/s for the first 17.5 hours of the experiment and was subsequently increased to 9.6 μm/s for the next 4.3 hours. In total, the experiment lasted 21.8 hours. Lidar scans were taken every 30 minutes during the low-uplift phase and every 20 minutes during the high-uplift phase. GoPro imagery was again used to observe individual events over the course of the experiment. The goal for experimental Run 3 was to emulate the success found in Run 2, while using a somewhat lower rock strength, thereby exploring this dimension of parameter space. Unfortunately, an error made during the sediment mixing process caused the substrate to behave differently than in Runs 1 and 2. Slightly less water was added while mixing the sand and clay together. While the resulting mixture was homogenous 4% clay by weight, it was not completely saturated. During the experiment, this unsaturated condition caused a fraction of precipitation to infiltrate the sediment package instead of behaving as surface runoff. The resulting 'groundwater' flow pattern created a localized discharge zone midway through the basin; high pore-fluid pressures in the discharge zone caused the landscape to destabilize after about 15 hours of run time.

Due to landscape destabilization, ridges failed to grow substantially, thereby limiting the ability to correlate ridge relief with sediment-discharge variability for both uplift rates. However, the observed sediment discharge (Q_s) for each uplift rate approached the theoretical steady-state value (set by uplift rate), regardless of pore-fluid induced destabilization. Further, the basin acquired a relatively natural looking, dendritic pattern with self-formed geomorphic processes like channel migration and stream captures, albeit with low relief (Figure 5.14).

Figure 5.14. GoPro imagery of the source terrane roughly 10 hours into Run 3. While there was less relief than expected, the terrane did develop a dendritic network of self-formed channels.

The most significant aspect of this run was the correlation observed between autogenic signals in the source and sink. Problems associated with imaging the sink terrane were resolved in the run, and I was able to capture sediment supply signals at the shoreline. This run provided confidence that the experimental apparatus works properly. As detailed below, sediment supply signals transmitted from the source correlated with shoreline progradation data in the sink.

Geomorphic Processes:

The lack of ridge relief and overall "mushiness" of the sediment package caused mass failures to occur in a regular, almost uniform flow, both spatially and temporally. Observing the terrane through GoPro imagery, it appears that the ridges shed entire layers of their "skin" over time, rather than through small, stochastic events. In a crude sense, the erosional drainage basin showed evidence of almost 'sheet like' flow of water and sediment. During both low- and high-uplift phases, average ridge relief was approximately 1.7 cm and 2 cm, respectively. Mean basin-wide relief was 0.21 and 0.29

49

cm, respectively. These values are similar to those observed during Run 1, when rock strength was low and the climate was wet (relatively high precipitation rate).

The source terrane was dissected by four to five main channels. While the channel valleys were not particularly wide, there was a high amount of channel migration within them, especially close to the outlet. These channels swept back and forth across their respective valley throughout the experiment, triggering small landslides on alternating ridges. Rivers quickly dispersed sediment supplied by mass failures. Numerous bars appeared and disappeared at different locations in the channels. Ultimately, these channels behaved more like alluvial rivers and less like bedrock channels. Notably, there was much less channel incision during this run than during Run 2.

Sediment Discharge:

During the low-uplift phase of the experiment, sediment discharge climbed gradually as the landscape appeared to approach a steady-state configuration (Figure 5.15). During this time interval, variability in Q_s was relatively low, likely reflecting the non-ideal behavior of the mechanically weak sediment package rather than the external parameters imposed on the system. Based on the physical appearance of the landscape and on the stabilization of sediment discharge, the basin appeared close to steady state at approximately 11.5 hours of run time; however, the observed mean sediment discharge at this time was only 66% of the theoretical discharge, indicating that the landscape had not reached dynamic equilibrium. When the tectonic uplift rate was tripled at $t = 17.5$ hours, there was an immediate spike in sediment discharge. Approximately two hours after the increase in uplift rate, sediment discharge began to stabilize at approximately 76% of the theoretical steady-state value. Unfortunately, this stable period was short-lived, as the unstable sediment package started to fail en-masse due to the high uplift rate forced on the basin.

The raw standard deviation (variability) in Q_s nearly quadrupled when uplift was tripled. When normalized to the observed sediment discharge, variability represented 7.2 and 7.8% of discharge at low uplift and high uplift, respectively. Using this method, variability was artificially large, because the system never reached true steady-state

during either phase of the experiment. When normalized to the theoretical steady-state sediment discharge, variability in Q_s was 4.7 and 6.0%, respectively. It is worth noting that while the system never reached a true steady-state, variability in Q_s (using all three methods) did increase when uplift was tripled.

In summary, the large-scale loss of mechanical strength in the basin substrate (the 'bedrock') due to high pore-fluid pressures during this run cast considerable uncertainty on the meaning of observed relationships between topographic relief, sediment discharge, and variability in sediment discharge. Observations from this experiment should be interpreted with caution. However, the erosional processes in the source terrane generated a sediment discharge that, while poorly understood, contained natural (autogenic) variability that was transferred to the attached sedimentary basin, i.e. the 'sink,' where they had the potential to drive fluctuations in the rate of fluvio-deltaic sedimentation.
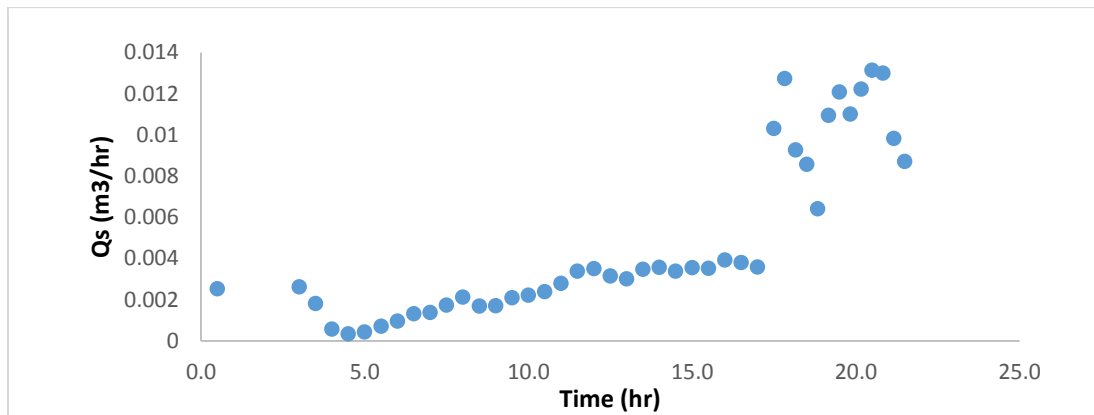

Figure 5.15. Time series of sediment discharge from the drainage basin during Run 3. Note that uplift was tripled at $t = 17.5$ hours.

Source-to-Sink Correlation

Experimental Run 3 provided the best shoreline data of all three runs. The experimental problems associated with imaging the shoreline were resolved for this run, allowing me to measure with certainty the shoreline progradation rate over time. Even though the conditions in the source terrane were not ideal, variability within the sediment supply signal existed throughout the run (i.e., sediment discharge was not constant). These variations in Qs—regardless of the details of their origin—provided an autogenic signal to the sink terrane. A digital camera captured images of the shoreline at one-minute

intervals. The mean position of the shoreline for each image was determined by averaging the left, center, and right positions of the shoreline. This was necessary due to channel migration that occurred near the delta front, which created an uneven shoreline. Next, shoreline progradation rates were determined by dividing average position change (i.e., distance) by the one minute-time interval. Finally, an average progradation rate was determined for its respective scanning period (30 minutes for low uplift, 20 minutes for high uplift) in order to have a single progradation rate to match with the corresponding sediment discharge during that interval (Figure 5.16). These 'matching' values were then tested for strength of correlation.
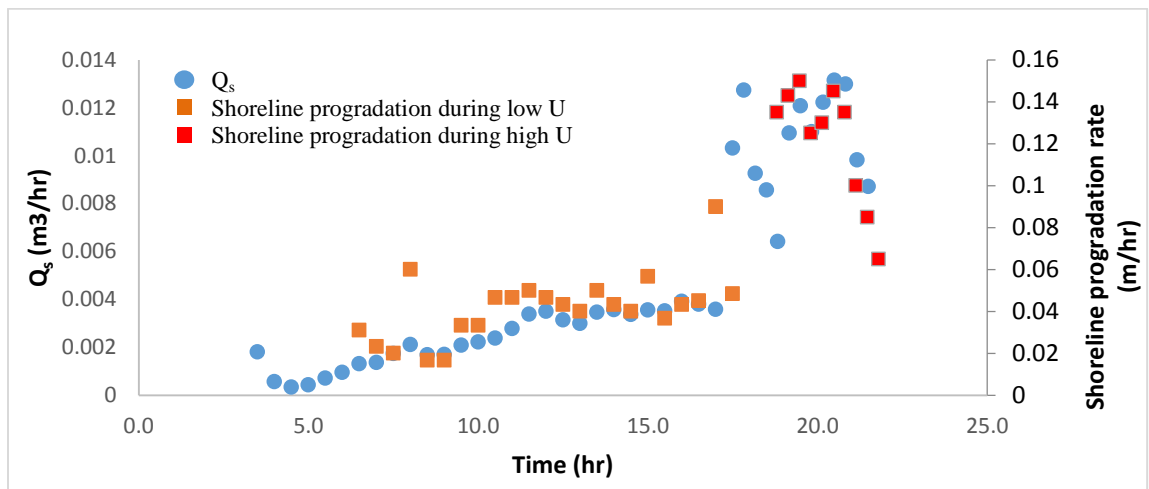

Figure 5.16. Time series of shoreline progradation rates (orange and red squares) and sediment discharge (Q_s, blue circles) from the drainage basin during Run 3. Shoreline progradation rates were determined by recording and observing average shoreline position through time.

The strength of correlation between sediment discharge and shoreline progradation rate at low uplift is displayed in Table 4. A direct comparison between the two results in a moderate positive relationship of 0.35. There is a very strong positive relationship of 0.80 when the shoreline is phase-shifted backwards by 30 minutes, i.e. progradation lags behind sediment discharge variability by approximately 30 minutes (or one scanning/measurement interval). This correlation suggests that the shoreline does a fairly decent job of capturing trends in sediment discharge data. In a general sense, shoreline

progradation rate does seem to imitate sediment yield from the source, yet there are limitations that arise when comparing the two sets of data. Both data sets feature data points that have been averaged over a 30 minute window. A single sediment discharge data point is the sum of dozens of landslides that have occurred between Lidar scans. Large bursts of sediment from the source terrane may have caused the shoreline to prograde rapidly at $t = 8$ hours and $t = 17$ hours, yet those bursts may have been lost through the averaging process. Shoreline progradation rates were also averaged over thirty minute periods, possibly filtering out individual progradation bursts. Another complication comes from lengthening of the depositional system with time. As the system grows, sediment yield signals have a greater potential to be filtered through temporary storage.

Low uplift		High uplift	
Shoreline time lag	Correlation coefficient	Shoreline time lag	Correlation coefficient
-30	0.27	-20	-0.13
0	0.35	0	0.46
30	0.80	20	0.35
60	0.24	40	0.04

Table 5.3. Correlation strengths for different shoreline time lags. A time lag of zero indicates a direct comparison between sediment discharge from the drainage basin and shoreline progradation rate measured over the same 20- or 30-minute interval. A negative time lag implies a lead, i.e. shoreline data was shifted backwards in time prior to calculating a correlation coefficient. A positive time lag implies shoreline data lagged sediment discharge data, i.e. shoreline data were shifted forward in time before calculating a correlation coefficient.
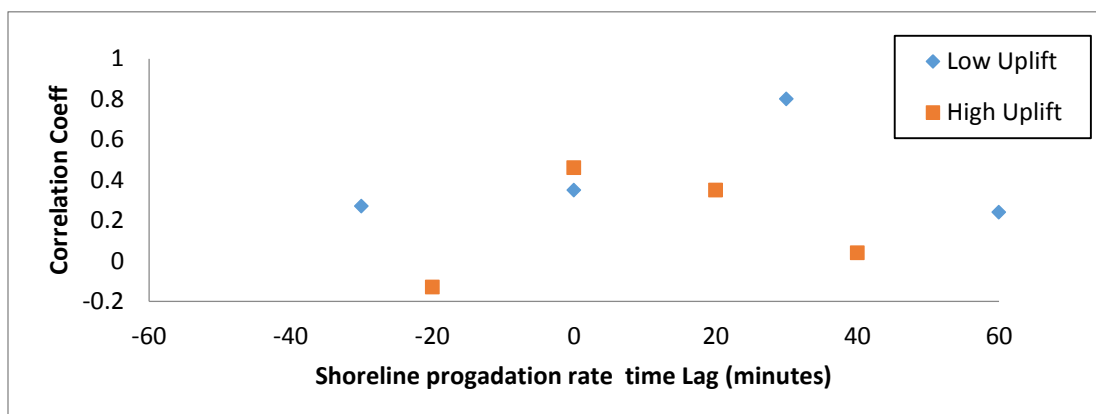
Figure 5.17. Correlation strengths for sediment discharge from the drainage basin and shoreline progradation rates for multiple shoreline time lags. (Note: Low-uplift-rate data employ a 30 minute lag/lead interval; high-uplift-rate data use a 20-minute interval.) At low uplift, the strongest correlation occurs when shoreline data were shifted 30 minutes forward in time. This suggests that the shoreline may have seen changes in sediment discharge from the basin roughly 30 minutes after the change occurred. At high uplift, the strongest correlation occurs when there is no time lag. This suggests changes in sediment discharge are felt almost immediately by the shoreline (during the same 20-minute interval).

At high uplift, sediment discharge and shoreline progradation have the best correlation when compared directly, without a shoreline phase shift (Table 5.4 and Figure 5.17). A positive relationship of 0.46 exists when compared directly and a moderate positive relationship of 0.35 exits when shoreline is shifted forward by 20 minutes (one scanning interval at high uplift). The lack of phase-shifting suggests the depositional basin captures signals from the source 'immediately', with little to no lag. The same limitations exist in this phase of the run, yet there seems to be little filtering done by the depositional system. It is possible that the tripling of total sediment yield during high uplift may have limited the amount of potential filtering within the depositional basin. In other words, there was so much sediment discharge exiting the source terrane that it 'overwhelmed' the sink and limited its ability to filter the source's signal.

Synthesis of autogenic variability

A *U/R* value in the source terrane has a direct positive relationship with variability in sediment discharge (Figure 5.18; upper panel). Increasing *U/R* in a landscape is

accomplished by increasing uplift or decreasing precipitation. Either of these scenarios results in an overall increase in characteristic ridge relief which, in turn, increases the size of potential mass failures that contribute to sediment yield variability from the source. Likewise, strong bedrock creates the potential for tall ridges with steep slopes, features that promote large mass failure events and, ultimately, high variability in the sediment yield signal. Figure 5.18 (lower panel) indicates that there is a direct positive relationship between rock strength (represented by clay content) and sediment discharge variability.

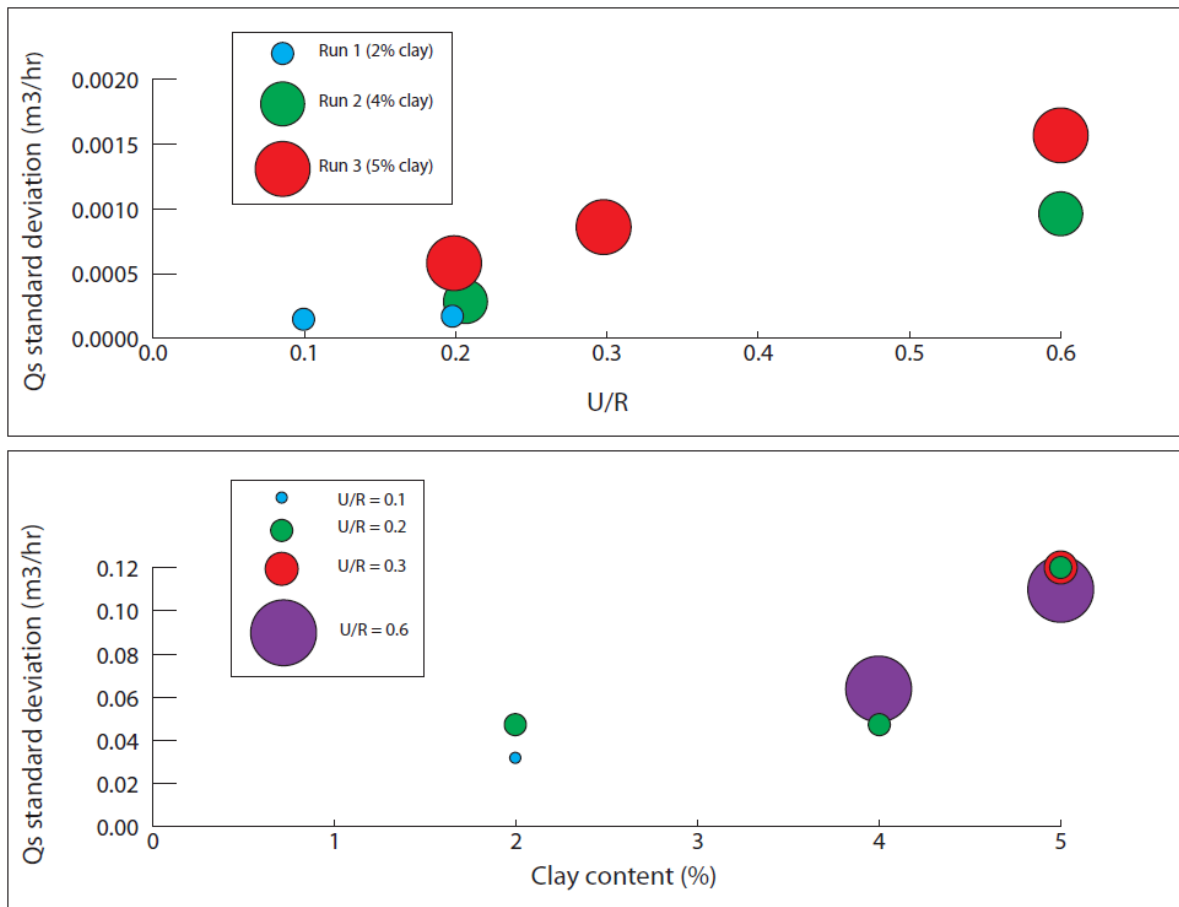**Figure 5.18**. Linear regression between variability in sediment discharge (δQ_s) and U/R values (upper panel; $R^2 \sim 0.78$) and clay concentrations (rock strength; lower panel; $R^2 \sim 0.76$). In the upper panel, the size of each data point represents clay concentration (rock strength). In the lower panel, point size represents U/R (the larger the point, the high U/R).

6. SUMMARY OF HYPOTHESIS TESTING

Section 3 (Problem Statement) laid out a series of hypotheses to be addressed with the above physical experiments; this section summarizes the experimental results in the context of these hypotheses. The three experimental runs, particularly Run 2, suggest a positive relationship between (raw or unscaled) autogenic variability in sediment discharge (δQ_s) and tectonics/climate (U/R; Fig. 5.18, upper panel) and rock strength (Fig. 5.18, lower panel). On the basis of these relationships, we must **reject** the null hypothesis (H_o: *The magnitude of fluctuations in sediment discharge (δQ_s) from the source terrane is independent of uplift rate, precipitation rate, or rock strength*). Likewise, in terms of raw variability in Q_s, the experimental results indicate that we cannot reject the alternative hypotheses (H_1 and H_2). That said, when the variability in Q_s is normalized with theoretical equilibrium sediment yield (UA), the dependency of δQ_s on U/R is less clear, suggesting that we may not be able to reject the 'normalized' equivalent of H_2. However, all 'forms' of δQ_s (raw, normalized) show a robust dependence on rock strength (clay content), indicating that we cannot reject H_3.

Experimental Run 3 addressed the issue of signal propagation and preservation at the shoreline. While somewhat less convincing than the relationships shown in Figure 5.18, the experiment suggests that information (the autogenic signal) from the source terrane is preserved in part at the shoreline. This 'preservation' is reflected in the correlation coefficient between sediment-discharge variability (δQ_s) and fluctuations in shoreline progradation rate (Fig. 5.17). On the basis of these observations, we must **reject** the null hypothesis (H_o: *Fluctuations in shoreline progradation rate are uncorrelated with fluctuations in sediment discharge*). The alternative hypothesis H_3 cannot be rejected, though the correlation between shoreline progradation rate and variability in Q_s is not particularly strong.

7. GEOMORPHIC AND STRATIGRAPHIC IMPLICATIONS

The results of this study would appear to have important implications for the interpretation of the sedimentary rock record. Currently, stratigraphers struggle to

disentangle 'traditional' autogenic signals—due primarily to avulsions in the fluvial system—from allogenic signals due to fluctuations in relative sea level or (less commonly) basin sediment supply. The results of this work would introduce an additional source of uncertainty or non-uniqueness to their interpretations—namely autogenic fluctuations in basin sediment supply that result entirely from internal dynamics in the 'external' source terrane. Scaling issues aside, the experimental results suggest that— under the 'right' conditions—autogenic fluctuations in sediment supply exceeding 10% of the equilibrium value set by tectonics ($Q_s = UA$) are plausible. A variation to basin sediment supply of this size would be sufficient to drive cycles of shoreline regression and transgression at the 'parasequence' scale in many fluvio-deltaic systems.

Results from this study suggest that variability in Q_s is maximized in drainage basins with rapid uplift rate and/or low precipitation rate (large U/R) and/or strong substrate (high clay content), i.e. in systems where relief is relatively large. In the natural systems, the 'right' conditions translate as tectonically active areas with relatively 'dry' climates and mechanically competent bedrock. Sedimentary basins adjacent to such systems would thus be most affected by autogenic variations Q_s, in principle.

But how plausible are the results of this study? Just how distorted is the scaling between the experimental basins and natural systems? It is difficult to connect the meaning of rock strength in natural systems with the clay content of the experimental substrate. The experimental values of U/R are quite distorted relative to natural systems: The experimental U/R values are order 10^{-1} to 10^{0}; in natural systems, a benchmark uplift rate is 1 mm/year, and a representative precipitation rate is 1 m/year, which together yield a U/R value on the order of 10^{-3} or smaller. It is difficult to determine how this distorted U/R value, in combination with essentially unconstrained scaling of rock strength, affects the scaling of landscape dynamics. While a rigorous statistical analysis of the drainage basin properties (e.g. relief, drainage density) was not the focus of this work, we can say that the drainage network 'appeared realistic' and generated hillslope-channel interactions that seemed physically plausible.

As Paola (2000) and Paola et al. (2009) note, it is important to remember that experiments like these are not intended to represent properly scaled 'simulations' of natural-scale systems. Rather, they are designed to gain insight into the behavior of self-organized, channelized systems responding to known external forcing. The drainage basin is free to form a network of channels and associated ridges that adjusts its net erosion rate to balance tectonic uplift. Furthermore, the sediment-discharge signal produced by this self-formed drainage basin is transmitted—unaltered—to depositional system free to build alluvial channels with self-formed width and slope connected to an avalanching delta foreset. In this admittedly distorted but self-organized system, autogenic processes in the source terrane appear to be transmitted to the shoreline, where they drive detectable fluctuations in progradation rate.

Intuitively, it would seem that autogenic sediment-supply signals would be most pronounced in relatively small drainage basins subject to high uplift rates and connected to depositional systems with small fluvial systems. Experimental results would suggest that the Q_s variability is maximized in these tectonically active systems and, further, that the resultant autogenic signal has a relatively good potential for propagation to the shoreline and preservation in the rock record. It turns out that such small, mountainous drainage networks play a disproportionally important role in the delivery of sediment to the modern global ocean (Milliman and Syvitski, 1992; Syvitski and Milliman, 2007). Assuming the importance of these small systems has been persistent over geologic time, perhaps autogenic variability in Q_s has been important in shaping the global sedimentary rock record.

The results of the full source-to-sink experiment (Run 3)—while not particularly robust—show relatively small time lags between variability in Q_s and variability in shoreline progradation rate. On the surface this would suggest that additional 'filtering' by the fluvial system is relatively minimal. An implication of this observation is that variability in the rock record is tied strongly to variability in the source terrane and less to autogenic processes in the fluvial system, i.e. it would suggest that the sort of 'signal shredding' processes studied by Jerolmack and Paola (2010) are somewhat less important in controlling variability in the rock record. A caveat to this claim is that the experimental

depositional system was small in scale, i.e. short, and lacking in some autogenic processes, particularly large-scale channel avulsion. However, the experimental fluvial system does have the potential to filter signals via aggradation / degradation in its upstream (proximal) section, *sensu* Marr et al. (2000) and Kim et al. (2006). Larger more complicated fluvial systems may filter and shred Q_s signals more effectively.

CITATIONS

Capart, H. et al. (2010) Formation and decay of a tributary-dammed lake, Laonong River, Taiwan, Water Resources Research, Vol. 46, Issue 11

Coulthard, T.J., Van De Wiel, M.J., 2013. Numerical modelling in fluvial geomorphology. In: Shroder, J. (Ed.), Wohl, E. (Vol ed.), Treatise in Geomorphology, Vol 9, Fluvial Geomorphology. Academic Press, San Diego, CA, US. pp. 694-710.

Hasbargen, L. E., and C. Paola (2000) Landscape instability in an experimental drainage basin, Geology, 28, 1067-1070.

Howard, A.D. (1994) A detachment limited model of drainage basin evolution, Water Resources Research, Vol. 30, No. 7, p. 2261 2285.

Jerolmack, DJ and Paola, C (2010) Shredding of environmental signals by sediment transport, Geophysical Research Letters, Vol. 37, L19401, p. 1-5

Lane (1955) The Importance of Fluvial Morphology in Hydraulic Engineering, Engineering Laboratories, Hydraulic Laboratories Report, Vol. 372

Liu, J.P. et al. (2008) Flux and Fate of Small Mountainous Rivers Derived Sediments into the Taiwan Strait. Marine Geology, Vol. 256, pp. 65-76.

Kim et al. (2006) Shoreline response to autogenic processes of sediment storage and release in the fluvial system Journal of Geophysical Research, Vol. 111

Marr et al. (2000) A two-diffusion model of fluvial stratigraphy in closed depositional basins. Basin Research, Vol. 12, p. 381-398.

Milliman, J.D., Syvitski, J.P.M. (1992) Geomorphic/tectonic control of sediment discharge to the ocean: the importance of small mountainous rivers. J. Geol. 100 (5), 525–544.

Paola, C et al. (1992) The large scale dynamics of grain-size variations in alluvial basins, 1: Theory. Basin Research, Vol. 4, p. 73-90.

Paola, C. (2000) Quantitative models of sedimentary basin filling: Sedimentology, Vol. 47, p. 121-178.

Paola, C., Straub, K., Mohrig, D, Reinhardt, L. (2009) The "unreasonable effectiveness" of stratigraphic and geomorphic experiments. Earth-Science Reviews. Vol 97. p 1-43.

Postma, G., Kleinhans, M.G., Meijer, P, and Eggenhuisen, J.T. (2008): Sedimentology, Vol. 55, Issue 6, p 1541-1557.

Schumm, S.A., Mosley, M.P., and Weaver, W. (1987) Experimental Fluvial Geomorphology. Regulated Rivers: Research & Management, Vol 2, Issue 5, p. 633-634.

Sheets et al. (2002) Assembling the stratigraphic record: depositional patterns and time-scales in an experimental alluvial basin. Basin Research, Vol 14, Issue 3, p. 287-301.

Swenson, J.B. et al. (2000) Fluvio-deltaic sedimentation: A generalized stefan problem. European Journal of Applied Mathematics, Vol. 11, Issue 5, p. 433-452.

Swenson, J.B. (2005) Fluviodeltaic response to sea level perturbations: Amplitude and timing of shoreline translation and coastal onlap. Journal of Geophysical Research: Earth Surface (2003–2012) 110 (F3)

Tucker, G.E., and G.R. Hancock (2010) Modelling landscape evolution. Earth Surface Processes and Landforms, 35(1): 28-50.

Visher, G.S. (1999) Stratigraphic Systems: Origin and Application. Academic Press. p 700.

Whipple, K. and Tucker, G., 1999, Dynamics of the stream power river incision model: Implications for height limits of mountain ranges, landscape response timescales and research needs: Journal of Geophysical Research, v. 104, no. B8, p. 17661-17674.

Appendix 1

Making a homogenous sand and clay mixture (~100 micron silica sand and Snow Brite brand kaolinite clay)

The procedure I am describing here has been developed through trial and error. I will explain what I have done wrong and what I have done right in an attempt to help others who plan on running an experiment similar to mine. Mixing sand and clay together seems easy enough, and it is. However, things get can definitely go wrong and if the mixture is not done correctly, you will be wasting a lot of time, money, and energy.

First, I tried dry-mixing the sand and clay together. I did this by hand (a drill with a cement mixer blade attachment) and in a large electric cement mixer. Upon 'mixing', the clay immediately separates itself from the sand by sticking to the walls of the container and the mixing blades (maybe it's because of the moisture in the air – I don't know) and by clumping up into balls. Also, lots of dry clay particles become airborne and coat the surrounding area in a thin film of clay. Not cool. Rebecca Eiden and I spent over two hours cleaning up clay from the Civil Engineering High Bay one Sunday afternoon.

Next, I decided to try wet-mixing. This is definitely the way to go. Still, proper mixing takes time and planning and is not as simple as combining all the ingredients together in a cement mixer. I first added the dry ingredients to the cement mixer, started it up, and then started spraying water from a hose into the mixture. It worked pretty well. Except I didn't know how much water I was adding and, in the end, there was a bunch of clay clumps in the mixture. It was not the smooth, homogenous mixture I was hoping for.

Then, I decided to mix clay and water together by hand (the drill with mixer attachment) before adding it to the sand. I mixed water and clay in a 5 gallon bucket until it was silky smooth. Then, I added the mixture into the cement mixer, where the dry sand was waiting. The amount of water used in the clay-water mixing process can vary. Basically,

you want to add enough water to the mixture to allow the clay to become smooth and non-clumpy. You'll probably end up needing to add more water to the sand-clay mixture, so you've got some flexibility here. Just be sure to keep track of how much clay you've added - I hesitate to report exact numbers here, because the size of sand, brand of clay, air moisture, gravitational pull of the moon, what you ate for lunch, etc. all play a role in how this thing works. However, I will tell you that I ended up making batches that consisted of 200lbs of sand, around 10lbs of clay (approximately 5%), and 10-15 liters of water. After you've added your clay-water mixture to the sand, start the cement mixer and let it run a while (5-10 minutes). Add water as needed to ensure full mixing and saturation (without over saturation - you don't want puddles of water forming in your mixture when you stop the cement mixer). I stopped the cement mixer every few minutes to sample the mixture. Once it wass well-mixed, smooth, and I couldn't see any clay clumps, I deemed it good to go. At this point, I would add the mixture, by the 5-gallon bucketful, into the basin. After loading, I let it sit overnight to settle out. With proper saturation, the mixture should 'flatten out' on its own. Any air pockets trapped within the package should release overnight, creating miniature air volcanoes on the surface.

Watch out for oversaturation of the mixture. Oversaturation will cause clay mobilization when you put the mixture into the basin. Basically, a pool of water will form on the top (with a bunch of clay in it). All the work you did to add the perfect amount of clay to the mixture is essentially ruined because there is now a whole bunch of clay sitting on the top (and not in the sediment package where it should be). It also causes unevenness in the sediment package. Under saturation is just as bad. A proper experiment will see the majority of precipitation being dedicated to surface runoff – this causes erosion and all of the cool features on the surface. Under saturation causes water to infiltrate the sediment package, which causes all sorts of complications in the way 'groundwater' behaves. When groundwater discharges to the surface, it creates instability, effectively destroying any features that have been created over the past 20+ hours. Fun.
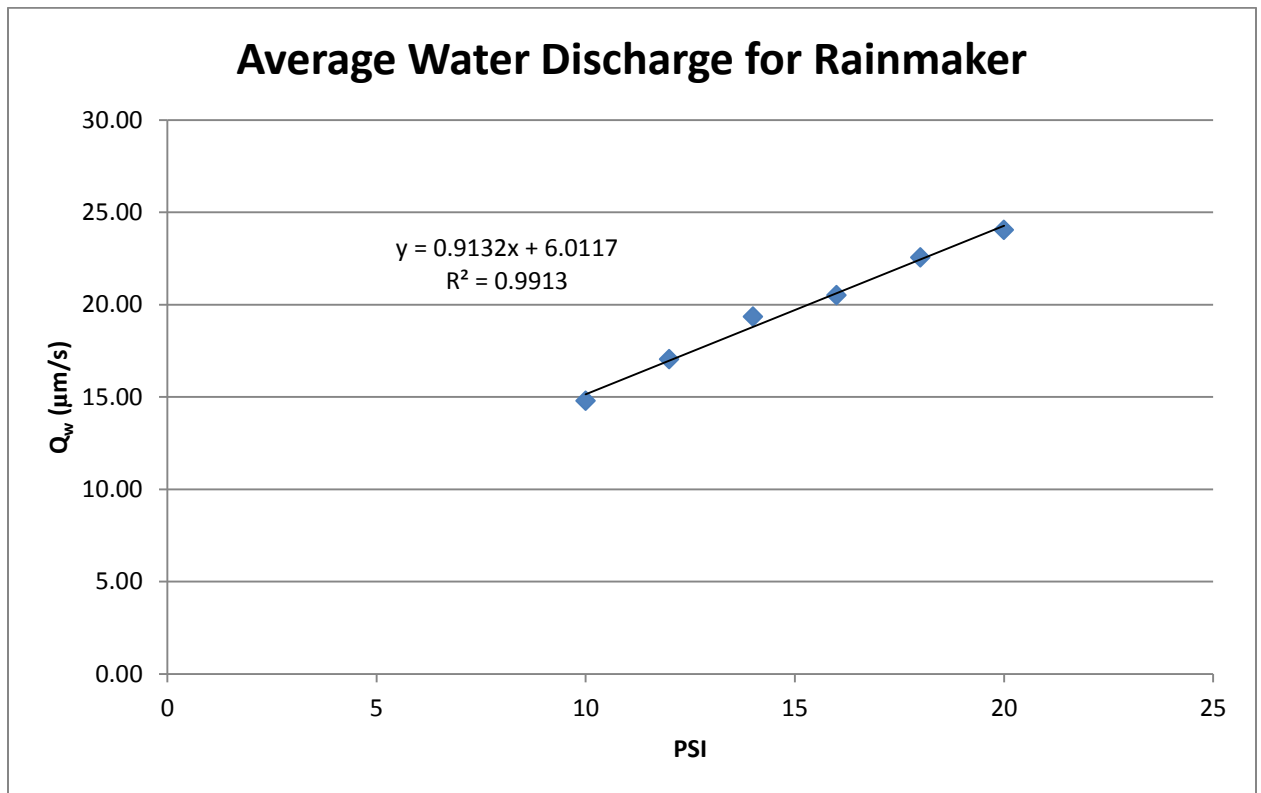
I can't stress enough that by the time I finished my experiments, I still hadn't perfected this process…so please take my words with due caution.

Appendix 2

Rainmaker water discharge

To determine water discharge rates for the rain maker, I used to following procedure (this procedure was done for the low ring open/upper ring closed configuration, as this is the only configuration used in this experiment):

The rain apparatus is controlled by a valve that regulates the amount of water spraying through its nozzles. A pressure gage behind the valve displays how much pressure is in the line. Pressure readings were used to set discharge rates throughout each experiment. To find out the discharge rate for a given pressure, I ran a set of experiments. First, I emptied out the drainage basin and covered it with a sheet of plastic. I secured the sheet to the basin, punched a hole in the center of it, and weighed it down to force all water towards the hole. Basically, I made a funnel on the top of the basin. Beneath the hole of the funnel, I placed a bucket to collect water. I ran the rainmaker for a minute at 12, 14, 16, 18, and 20 psi. Then, I measured the amount of water collected in the bucket for each pressure. I did this process three times. The average precipitation rates for each pressure are shown below.

Average Water Discharge for Rainmaker

$$y = 0.9132x + 6.0117$$
$$R^2 = 0.9913$$

Chart: Q_w (µm/s) versus PSI. Y-axis Q_w (µm/s) ranges from 0.00 to 30.00. X-axis PSI ranges from 0 to 25.

Appenidx 3

Finding an appropriate U/R for your system:

I spent a lot of time walking around in parameter space during this project. Finding the appropriate combination of uplift, rainfall, and clay content is tricky. I don't think I have perfected yet but I do know that you want to keep rainfall relatively low. Too much water, no matter how fast your uplift rate or how strong your sediment package is, will cause havoc. I settled in on a rainfall rate of 10-17 µm/s. The lower the better, especially because the Velmex motor (uplift) provides lots of flexibility with available uplift rates. A good 'low' uplift rate is around 1.15 cm/hr (40 steps per second in Velmex talk). Clay content is something I struggled with but overall, I think somewhere between 2-5%, when mixed properly, is a good window to work in.

When starting a run, I think it's a good idea to let a drainage basin develop at a relatively low uplift rate. If you turn uplift to a high rate right from the beginning, your landscape will develop large cliff faces (knickpoints) that take a very long time to migrate upstream.